Review

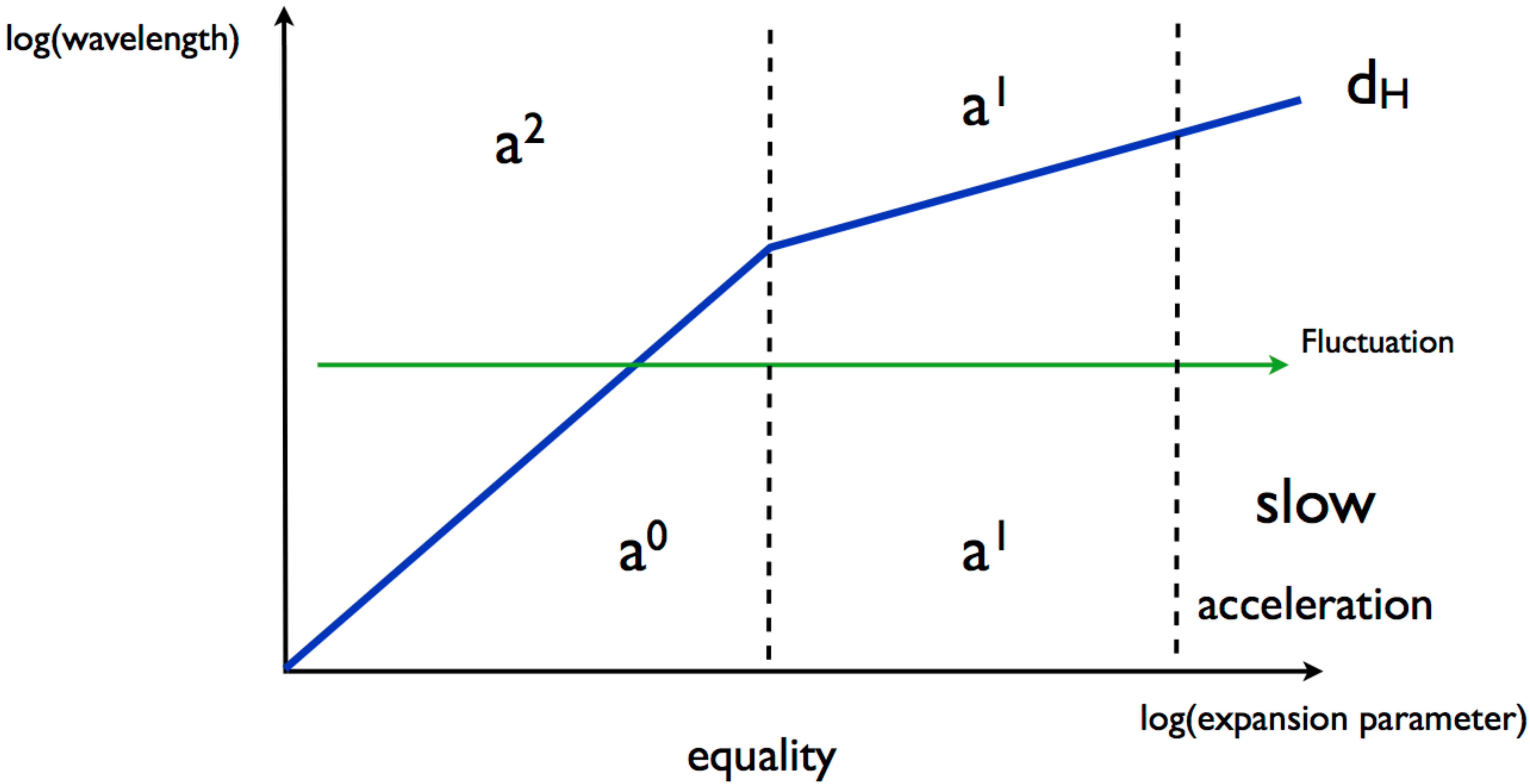

Chessboard of growth of adiabatic perturbations

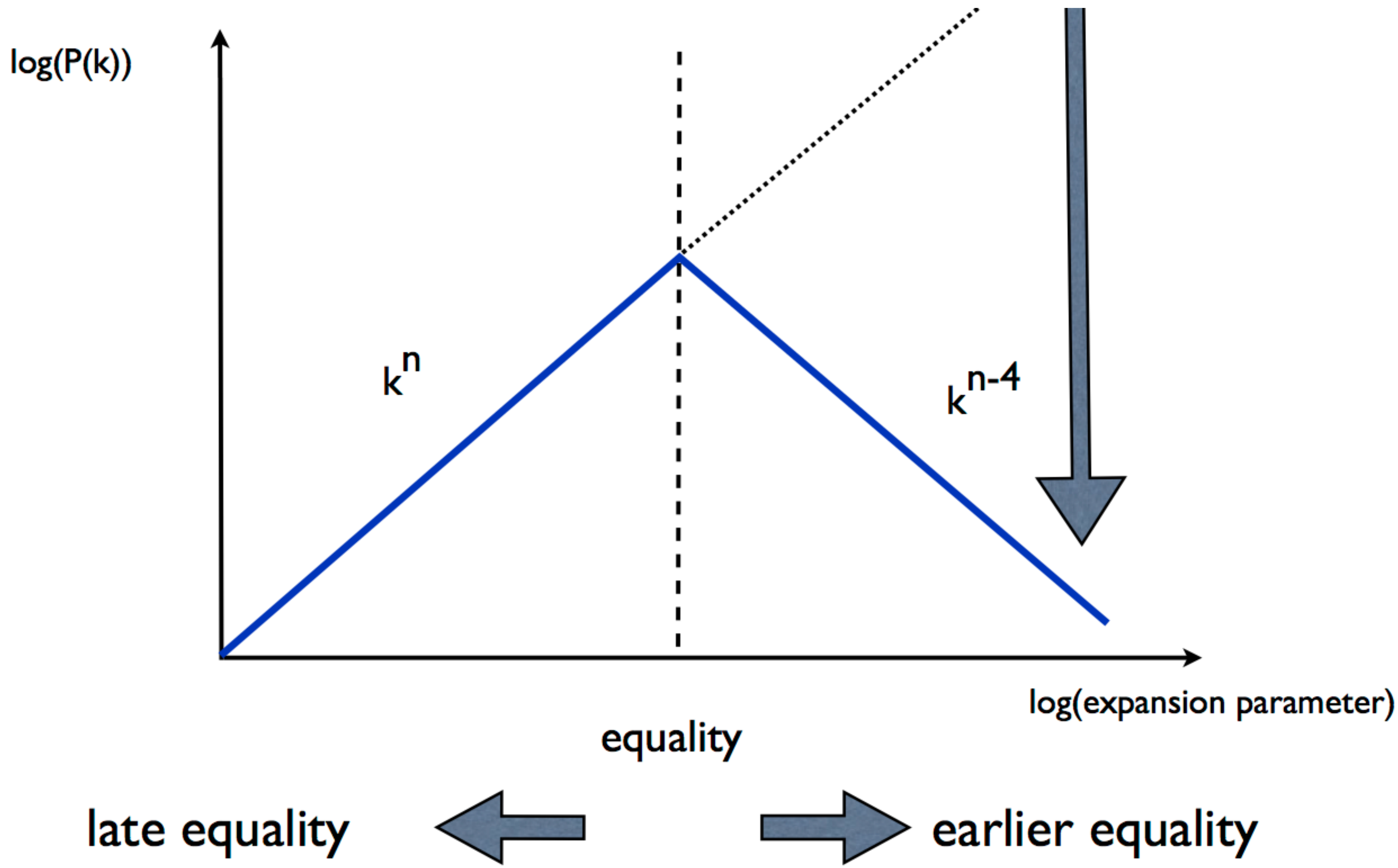

Power spectrum evolution

Power Spectrum

Consider a filed of density perturbations in a volume V

$$\delta(\vec{x}) = \frac{\rho(\vec{x}) - \rho_b}{\rho_b}$$

The average of the density contrast is equal to zero:

$$\langle \delta(\vec{x}) \rangle = 0$$

Let's find the dispersion of the density contrast: $\langle \delta^2(\vec{x}) \rangle$

Decompose the density contrast into the Fourier spectrum

$$\delta(\vec{x}) = \frac{V}{(2\pi)^3} \int d^3k \, \delta_{\vec{k}} \, e^{-i\vec{k}\vec{x}}$$

$$\delta_{\vec{k}} = \frac{1}{V} \int d^3x \, \delta(\vec{x}) \, e^{i\vec{k}\cdot\vec{x}}$$

$$\xi(r) = \frac{1}{2\pi^2} \int_0^\infty k^2 dk \, \frac{\sin kr}{kr} P(k)$$

There is an inverse relation:

$$P(k) = 4\pi \int r^2 dr \, \xi(r) \, \frac{\sin kr}{kr}$$

Dependance of P(k) on Ω_{matter}
Amplitude of fluctuations and $\Omega_{baryons}$ are fixed.

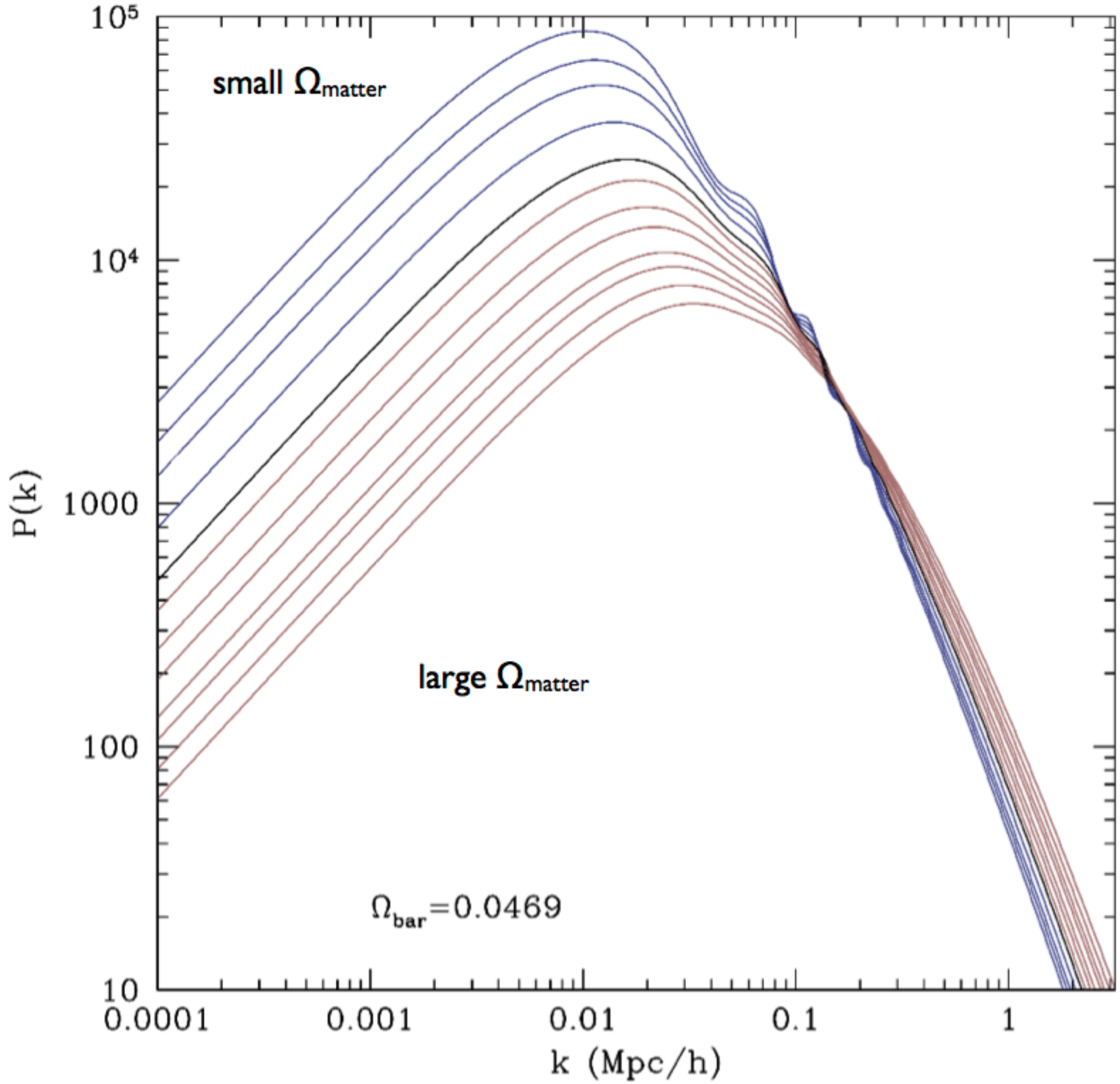

Dependance of Correlation function on Ω_{matter}
Amplitude of fluctuations is fixed at 5Mpc/h

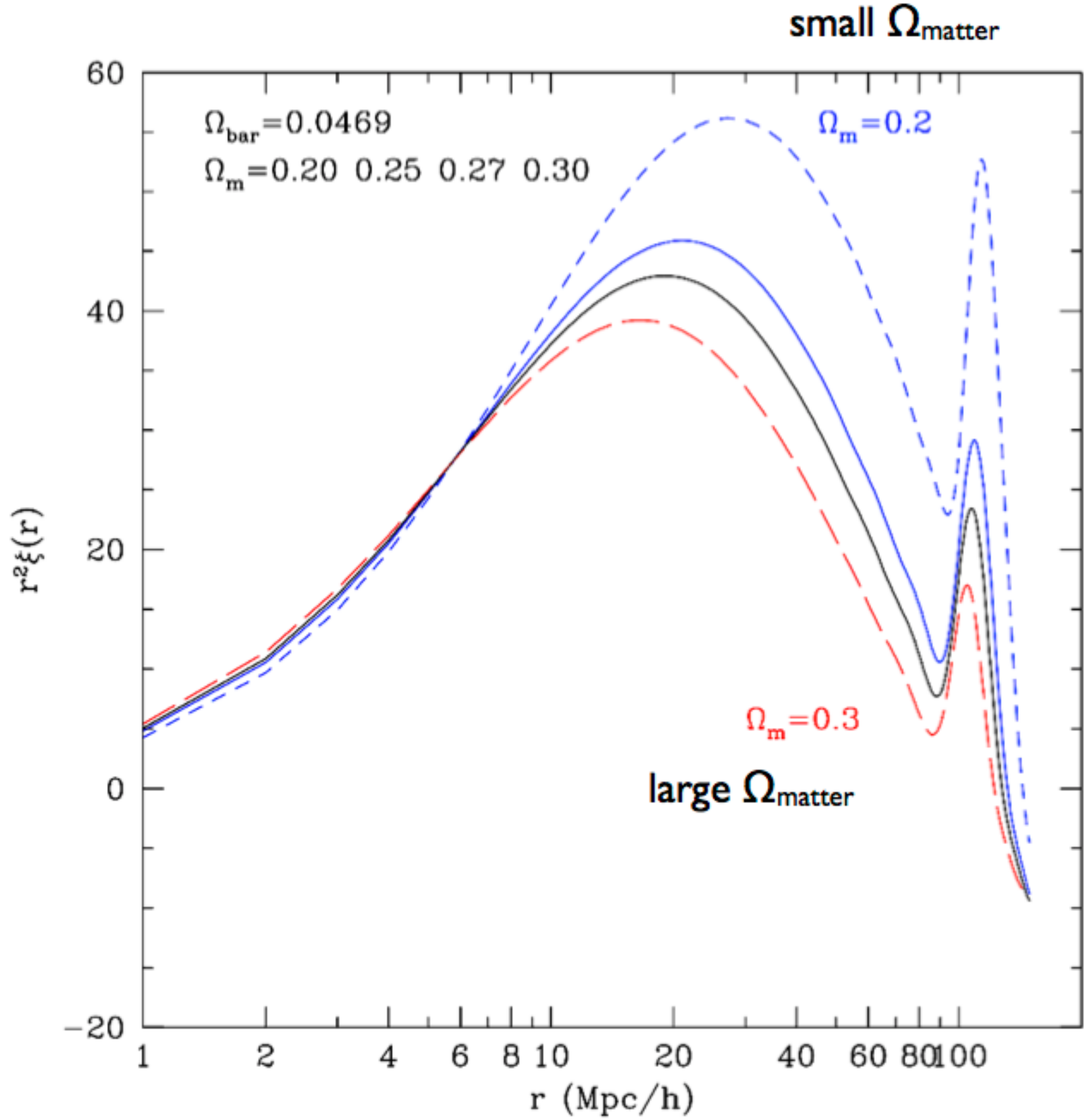

Dependance of Correlation function on $\Omega_{mbaryon}$
Amplitude of fluctuations is fixed at 5Mpc/h

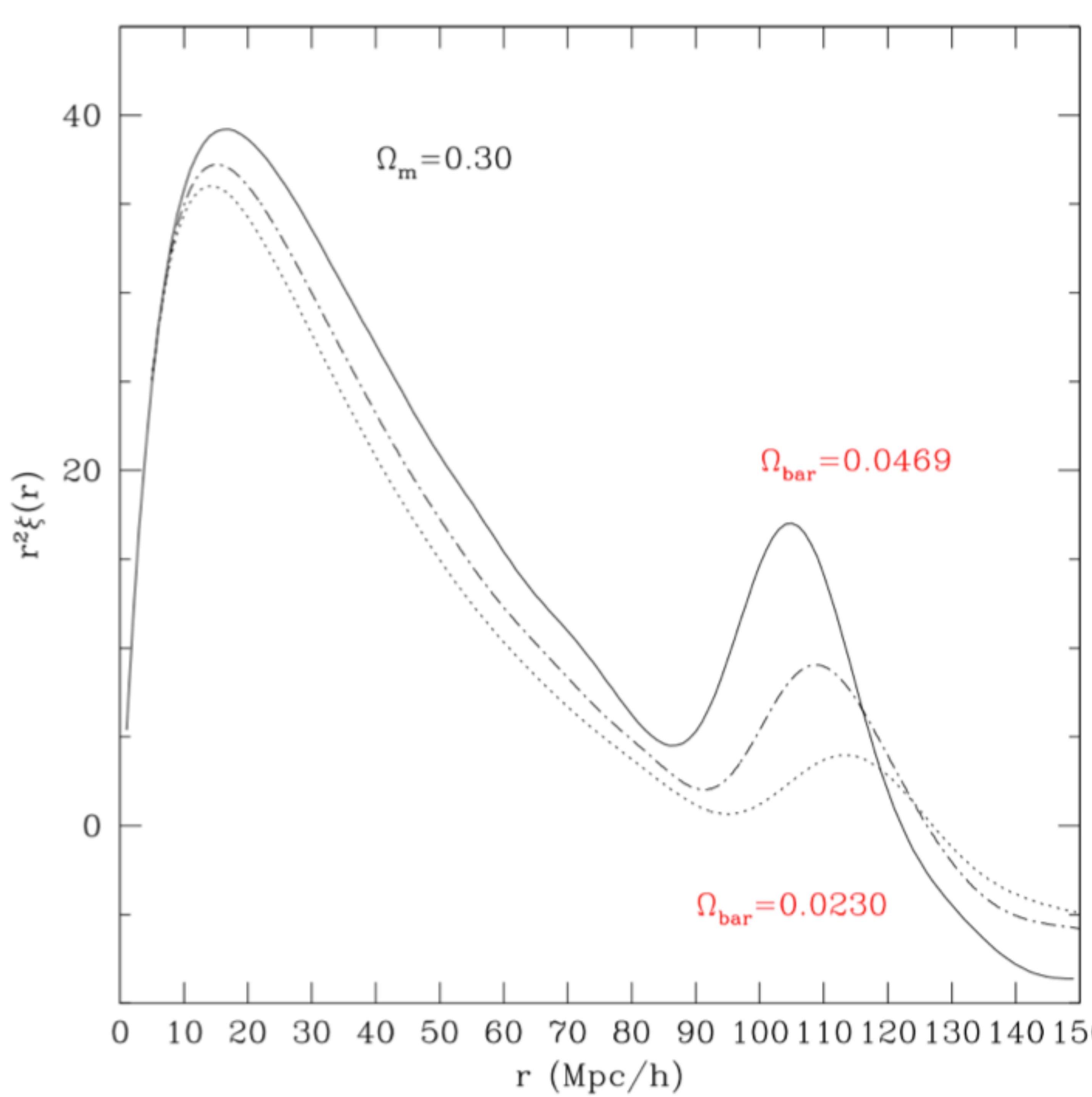

Following text is taken from S.Borgani lecture: http://fisica.usac.edu.gt/public/curccaf_proc/borganihtml/node4.html

The Zeldovich approximation

A simple and elegant approximation to describe the non-linear stage of gravitational evolution has been developed by Zeldovich [38] (see the review by Shandarin & Zeldovich [28], for an exhaustive description of the Zeldovich approximation). In this approach, the initial matter distribution is considered to be homogeneous and collisionless. If the unperturbed (initial) Lagrangian coordinates of the particles are described by $\mathbf{q}$, then the Eulerian coordinates of the particles at the time t are given by

$$\mathbf{r}(\mathbf{q},t) \;=\; a(t)\,[\mathbf{q}+b(t)\,\mathbf{s}(\mathbf{q})]\,. \tag{15}$$

Here $a(t)$ is the cosmic expansion factor and $b(t)$ the growing rate of linear fluctuations, as provided by eq.(13). Moreover, the velocity term $\mathbf{s}(\mathbf{q})$, which provides the particle displacement with respect to the initial (Laplacian) position, is related to the potential $\Phi_o(\mathbf{q})$ originated by the initially linear fluctuations, according to

$$\mathbf{s}(\mathbf{q}) \;=\; \nabla\Phi_o(\mathbf{q})\,. \tag{16}$$

In order to better visualize the meaning of eq.(15), let us consider a pressureless and viscosity-free, homogeneous medium without any gravitational interaction. For this system, the Eulerian positions $\mathbf{x}$ of the particles at time t are related to the Lagrangian positions $\mathbf{q}$ by the linear relation

$$\mathbf{x}(\mathbf{q},t) \;=\; \mathbf{q}+\mathbf{v}(\mathbf{q})t\,, \tag{17}$$

being $\mathbf{v}(\mathbf{q})$ the initial velocity. The above expression is essentially analogous to the Zeldovich approximation (15), apart from the presence of the $a(t)$ term, which accounts for the background cosmic expansion, and of the $b(t)$ term, which accounts for the presence of gravity, giving a deceleration of particles along the trajectories (actually, $b(t)\propto t^{2/3}$ in a $\Omega=1$ matter dominated Universe).

Since at $t>0$ density inhomogeneities are created, mass conservation requires that $\rho(\mathbf{r},t)\,d\mathbf{r}=\rho_o\,d\mathbf{q}$, so that the density field as a function of Lagrangian coordinates reads

$$\rho(\mathbf{q},t) \;=\; \rho_o\left|\frac{\partial\mathbf{r}}{\partial\mathbf{q}}\right| \;=\; \frac{\bar{\rho}}{\left|\delta_{ij}-b(t)\,\frac{\partial s_i}{\partial q_j}\right|}\,. \tag{18}$$

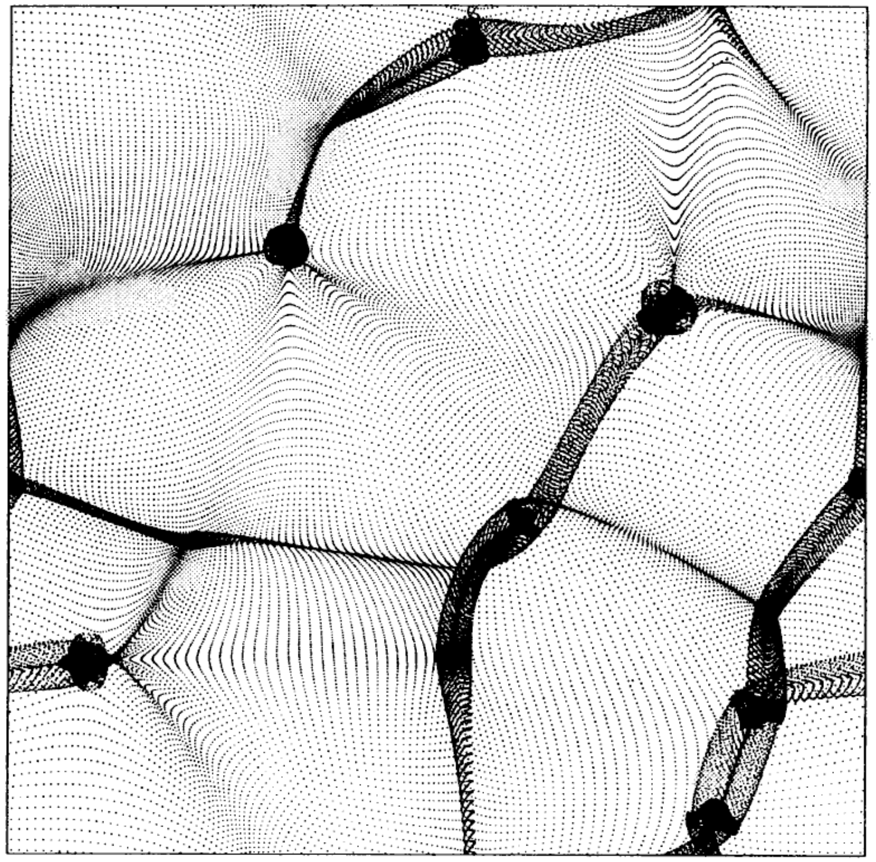

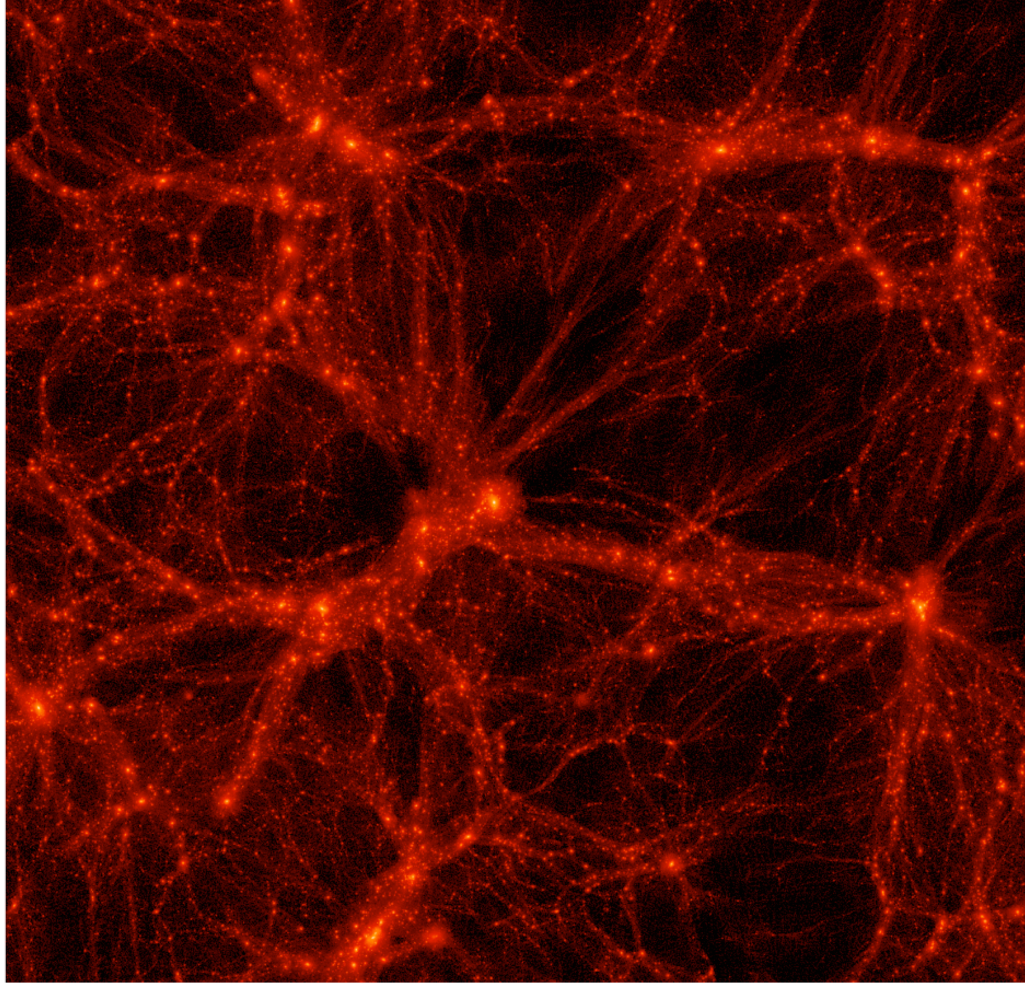

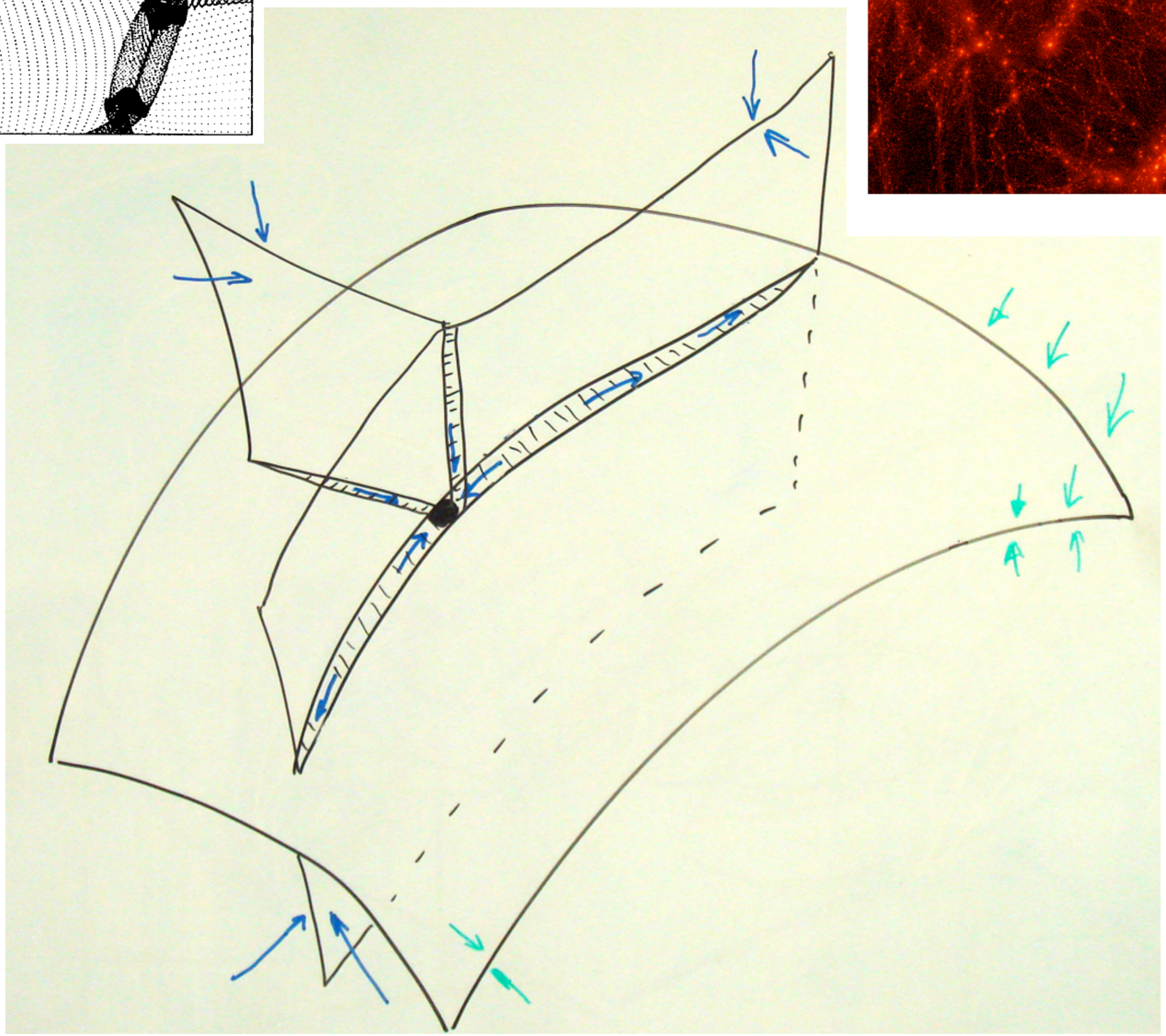

Properties of DM halos: statistics

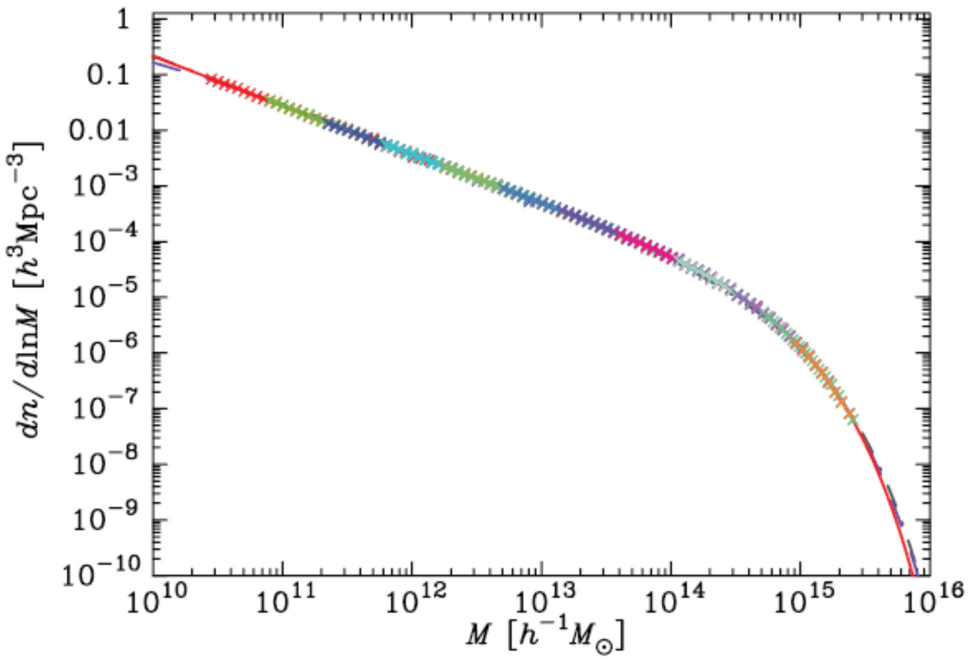

dn/dM~M^{-2}

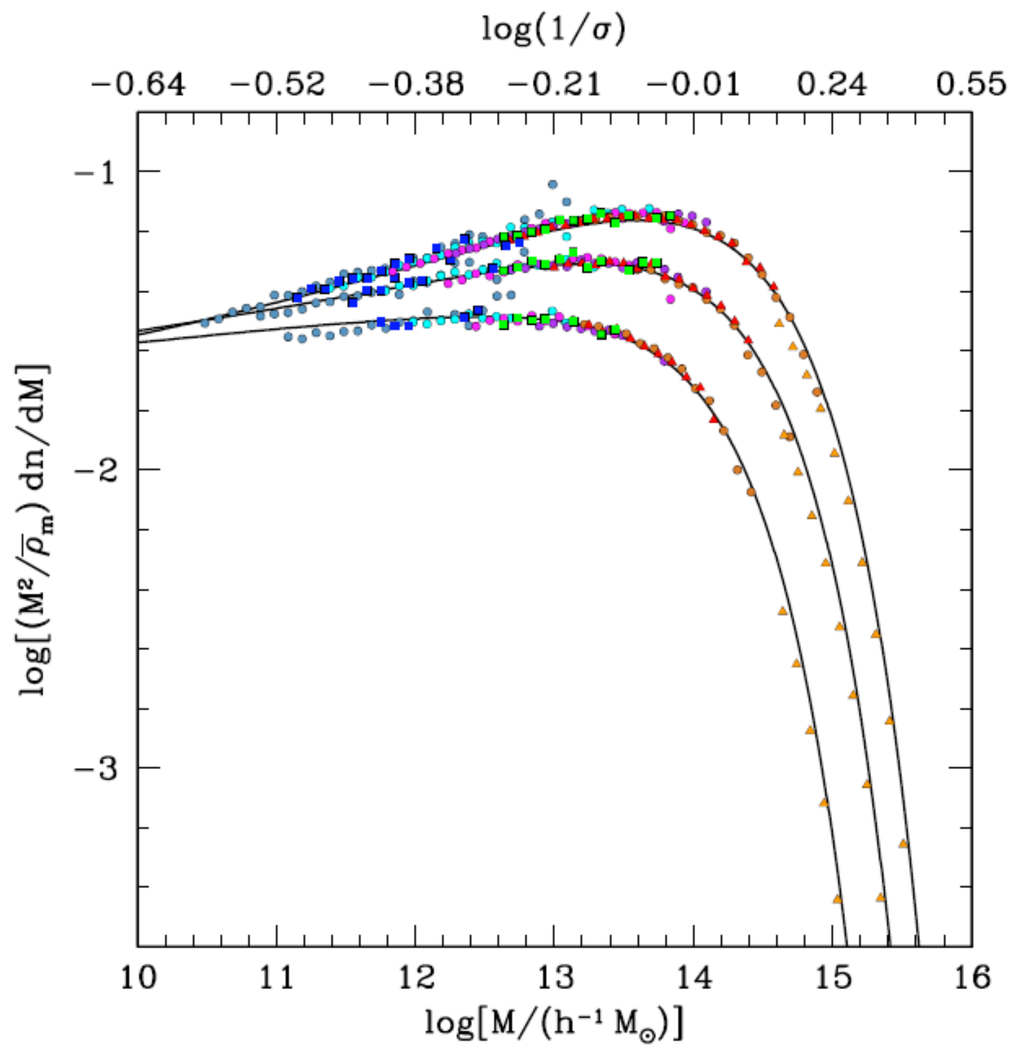

$$\frac{dn}{dM} = f(\sigma)\,\frac{\bar{\rho}_m}{M}\,\frac{d\ln\sigma^{-1}}{dM}$$

$$\sigma^2(M) = \frac{b^2(z)}{2\pi^2}\int_0^\infty k^2 P(k) W^2(k;M)\,\mathrm{d}k,$$

Evolution of the mass function with redshift

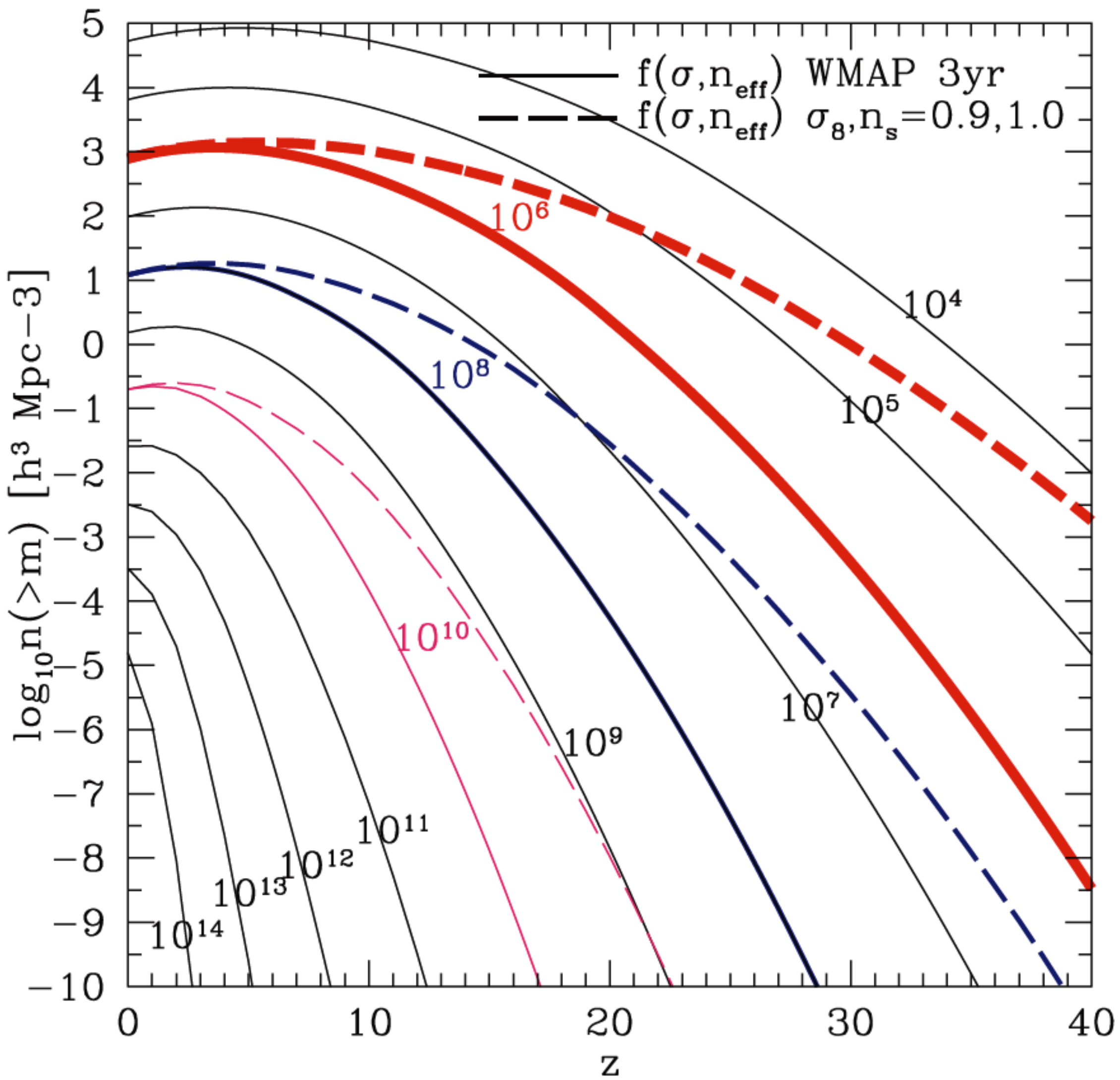

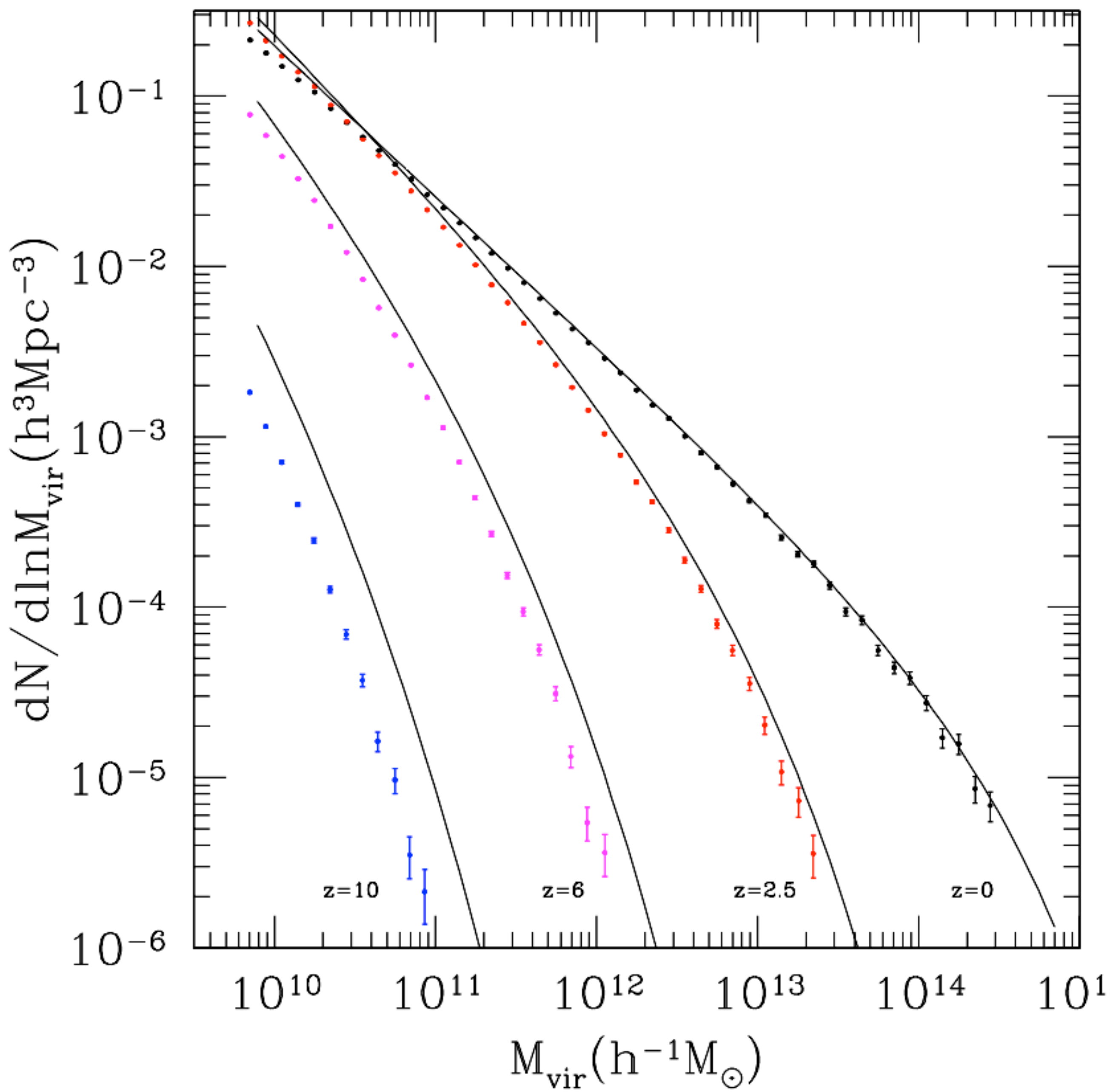

Properties of DM halos

Concentrations: different regimes of halo growth

$$c(M_{\rm vir}) = 9.60 \left(\frac{M_{\rm vir}}{10^{12}\,h^{-1}\,M_\odot} \right)^{-0.075}$$

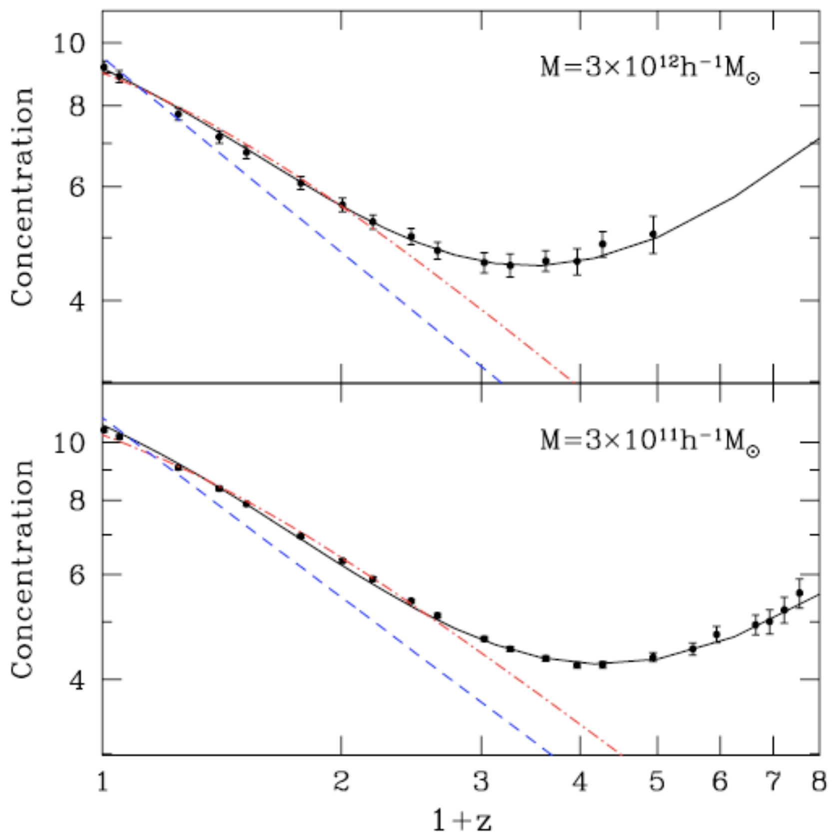

Figure 6. Evolution of halo concentration for halos with two masses indicated on the plot. The dots show results of simulations. For the reference the dashed lines show a power-law decline $c \propto (1+z)^{-1}$. Concentrations do not change as fast as the law predicts. At low redshifts $z < 2$ the decline in concentration is $c \propto \delta$ (dot-dashed curves), where δ is the linear growth factor. At high redshifts the concentration flattens and then slightly increases with mass. For both masses the concentration reaches a minimum of $c_{\rm min} \approx$ 4–4.5, but the minimum happens at different redshifts for different masses. The full curves are analytical fits with the functional form of Equation (13).

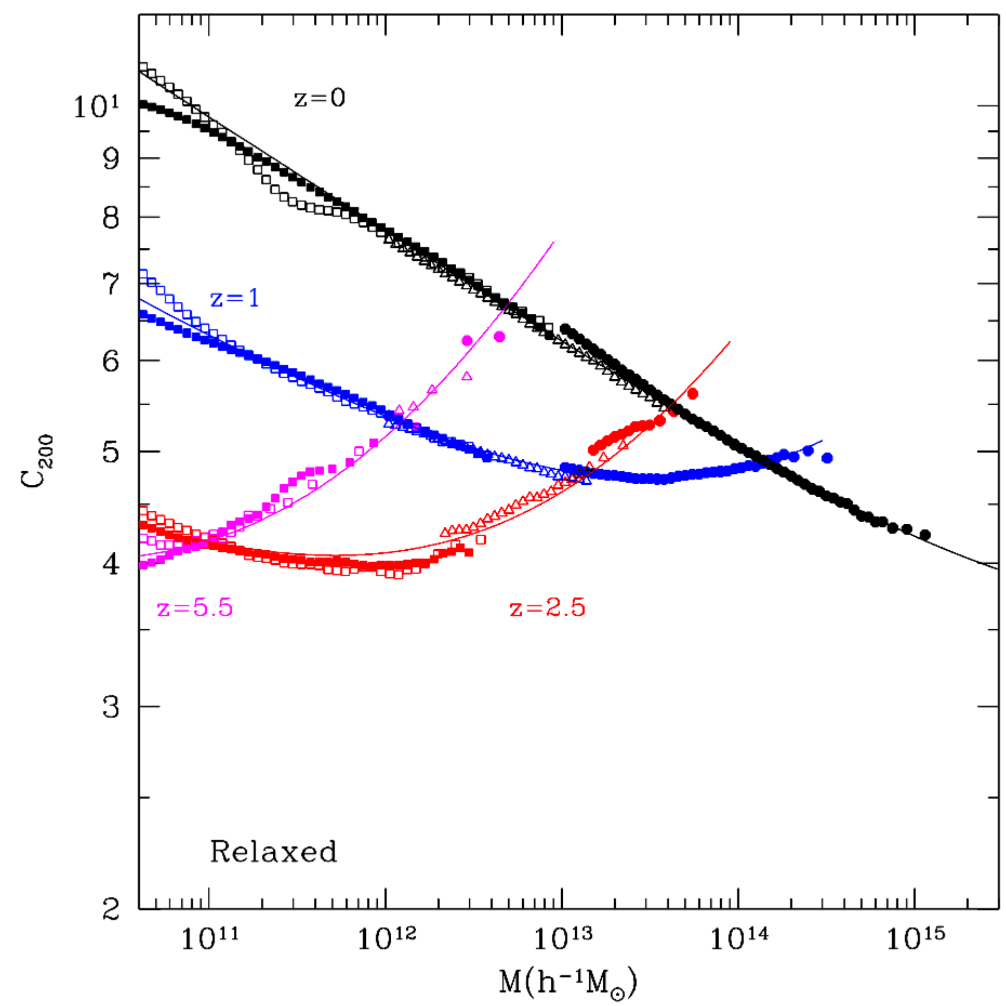

Properties of DM halos

Structure of halos

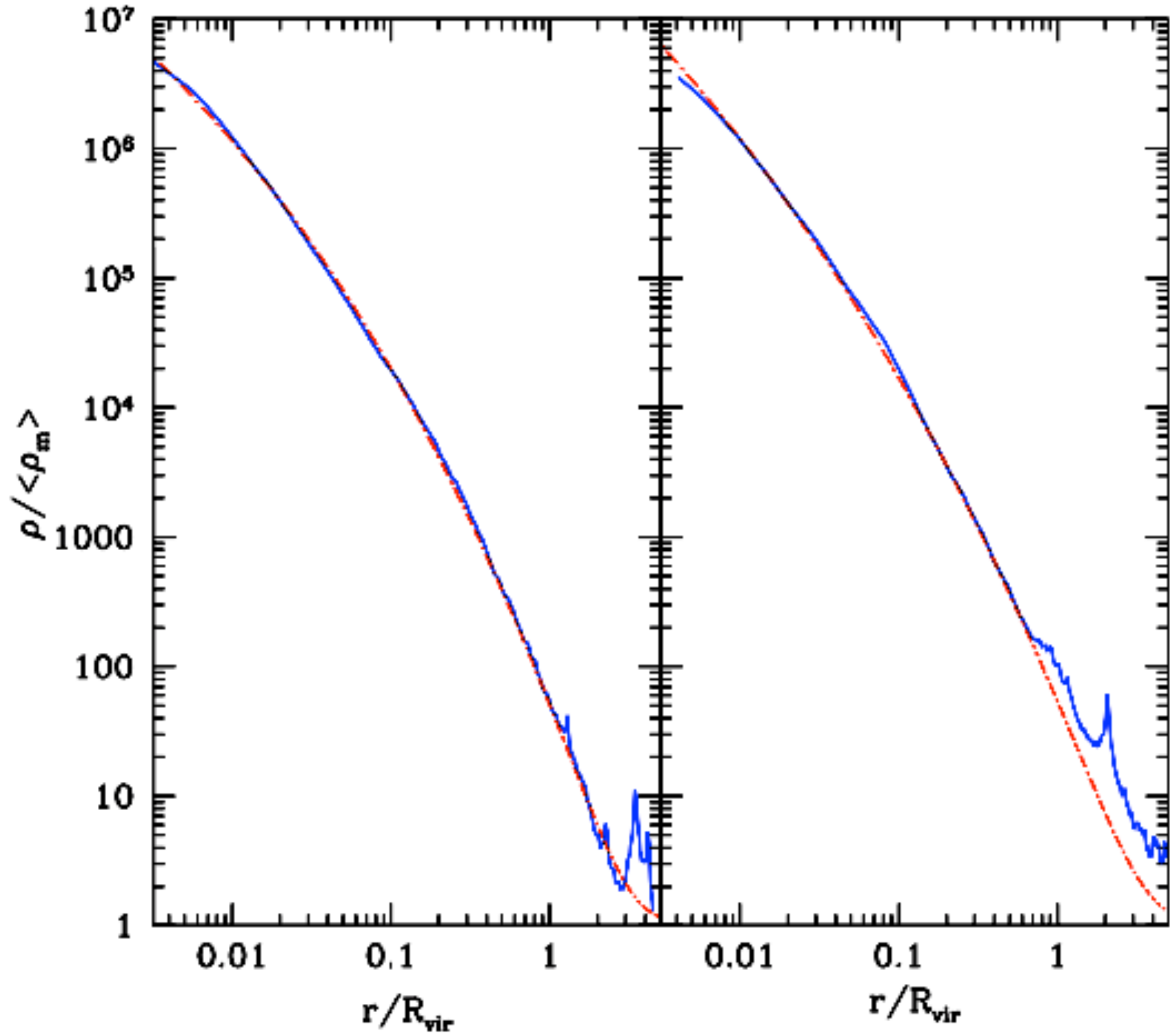

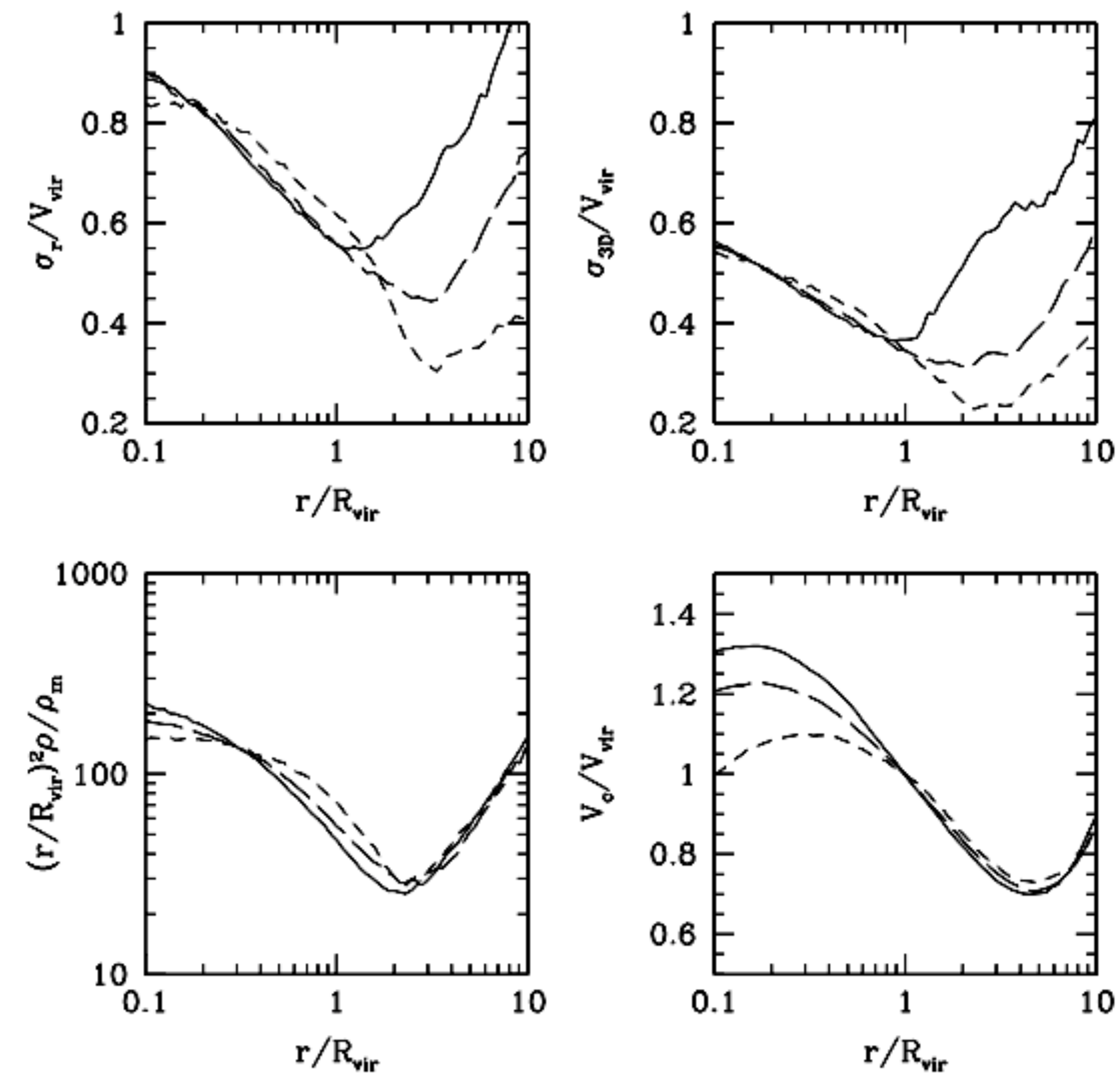

Properties of DM halos

Structure of halos

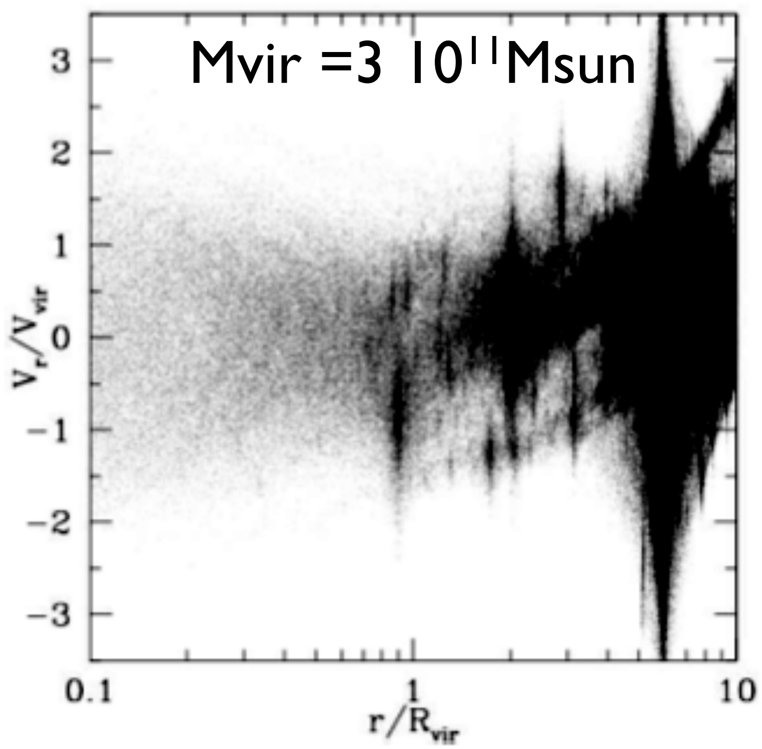

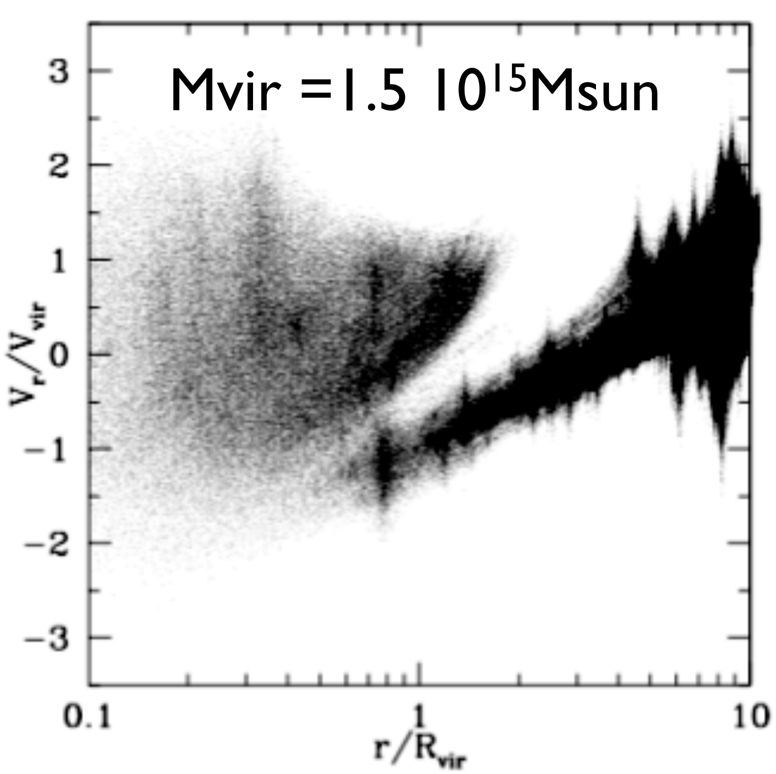

Phase-space diagram for the particles in dark matter halos

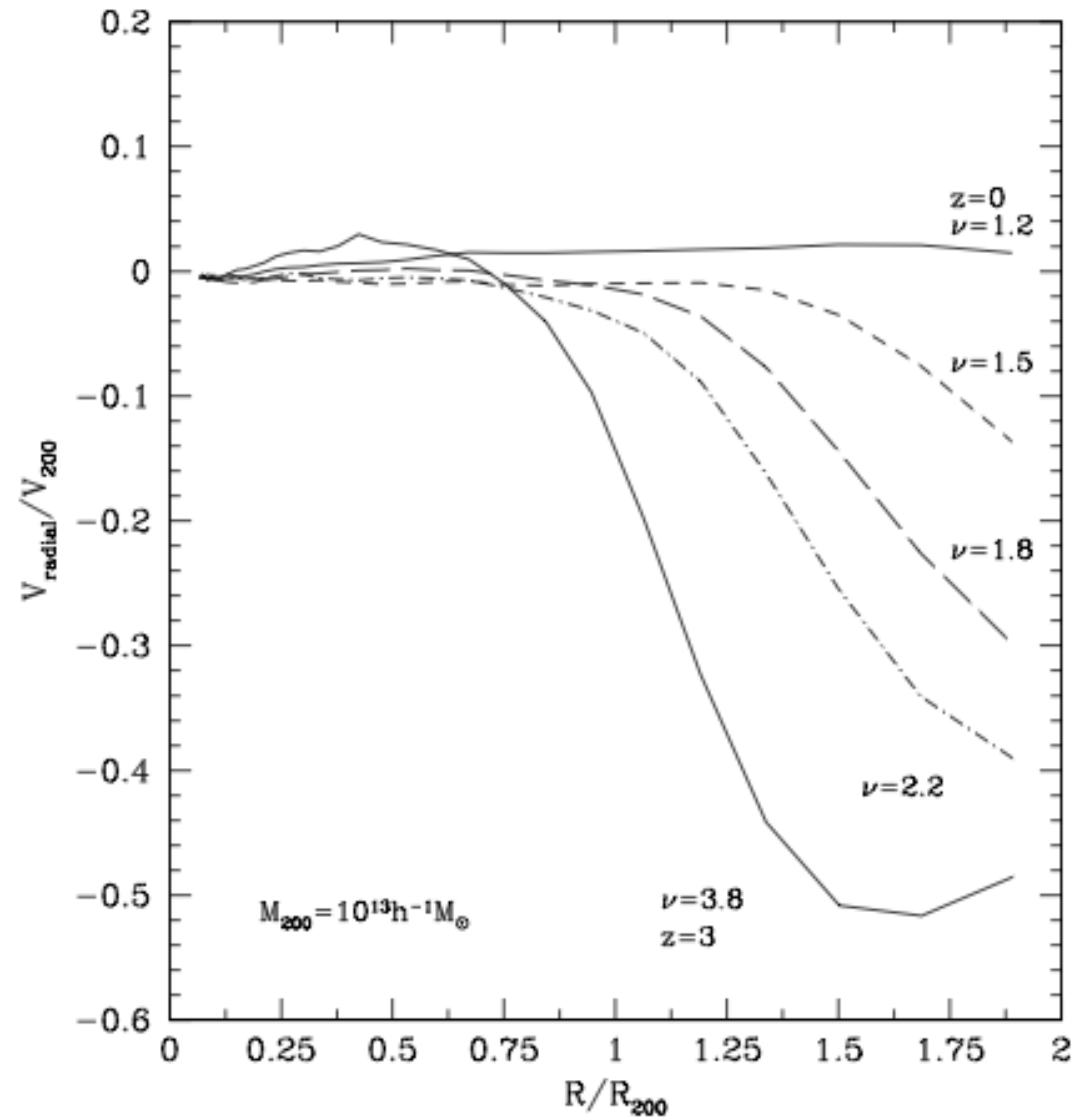

Structure of halos

Velocity anisotropy

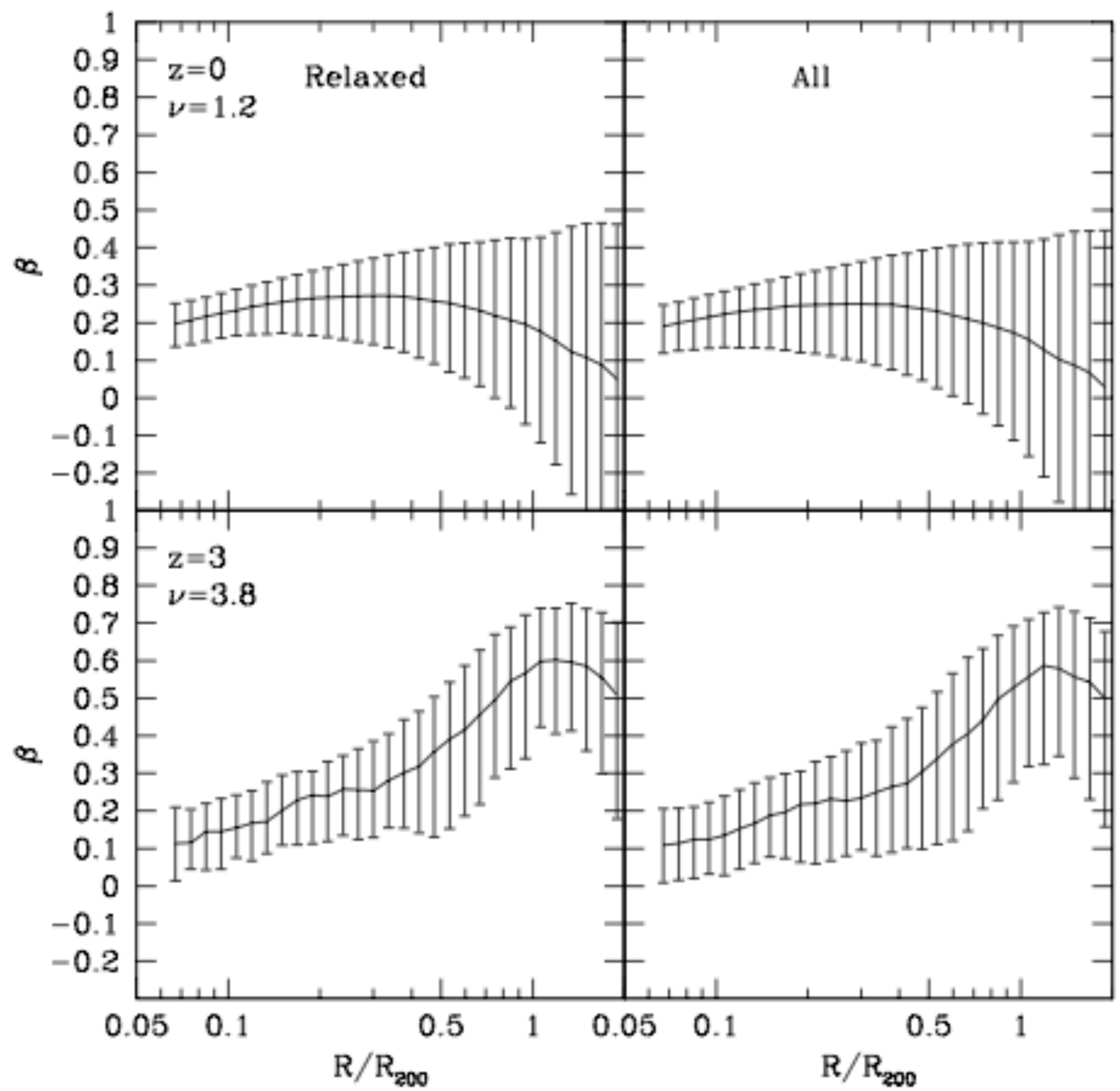

Cold Flows

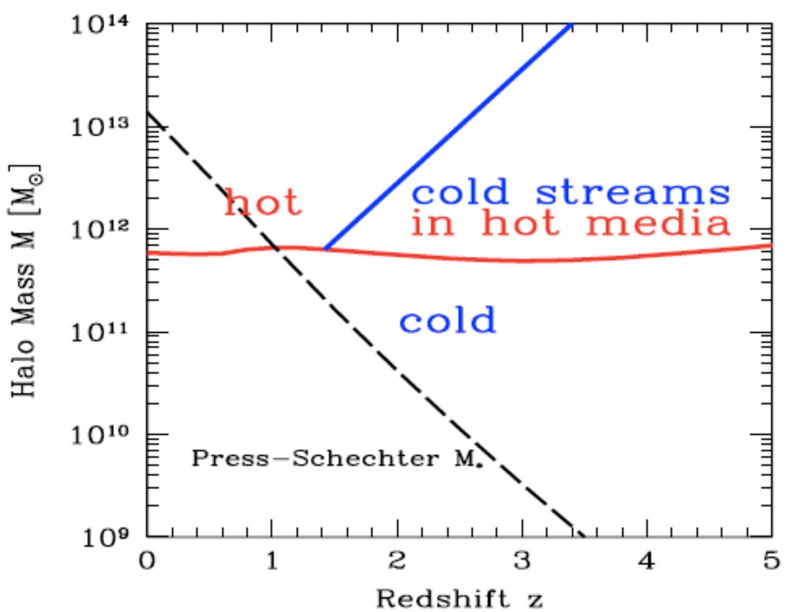

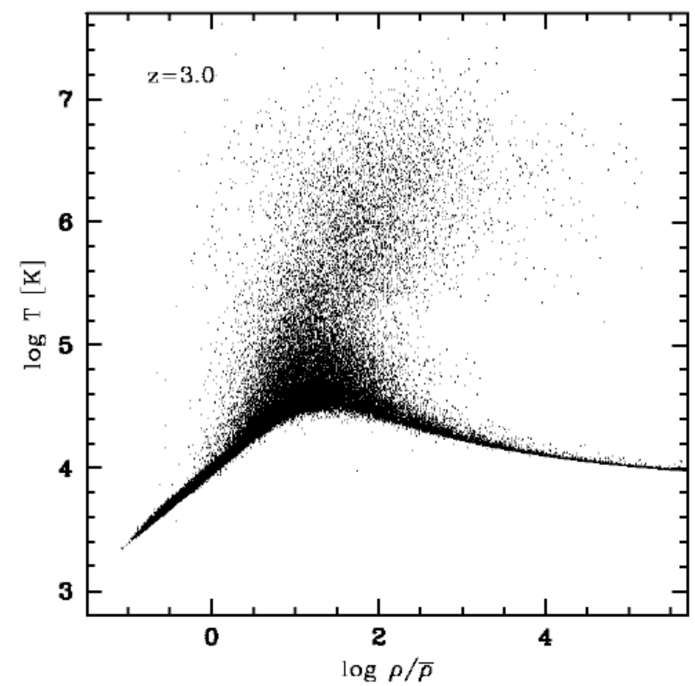

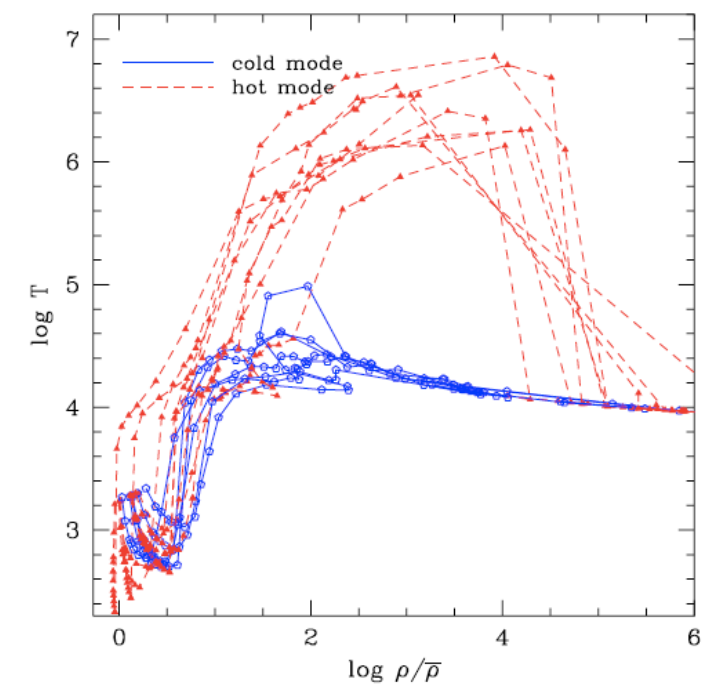

We investigate the conditions for the existence of an expanding virial shock in the gas falling within a spherical dark-matter halo. The shock relies on pressure support by the shock-heated gas behind it. When the radiative cooling is efficient compared to the infall rate the post-shock gas becomes unstable; it collapses inwards and cannot support the shock. We find for a monoatomic gas that the shock is stable when the post-shock pressure and density obey

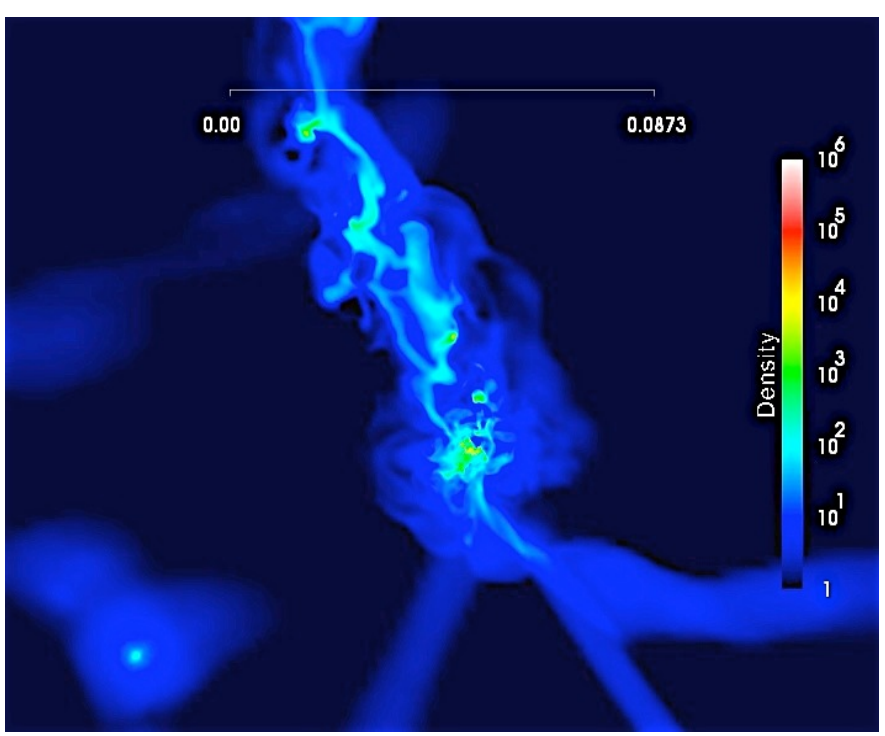

Flattening of cusps due to multiple bursts of SF

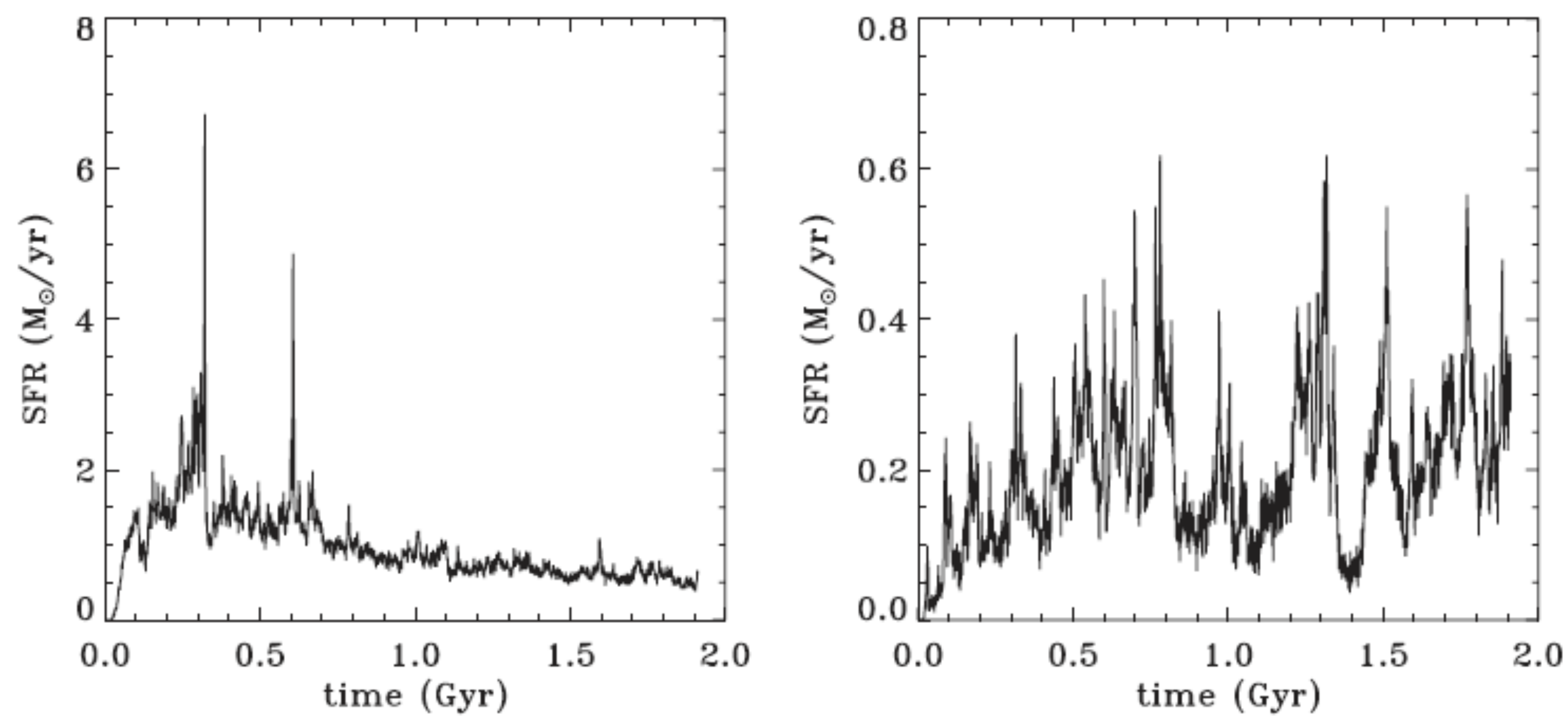

Figure 3. Star formation history in the runs without (left-hand plot) and with (right-hand plot) feedback.

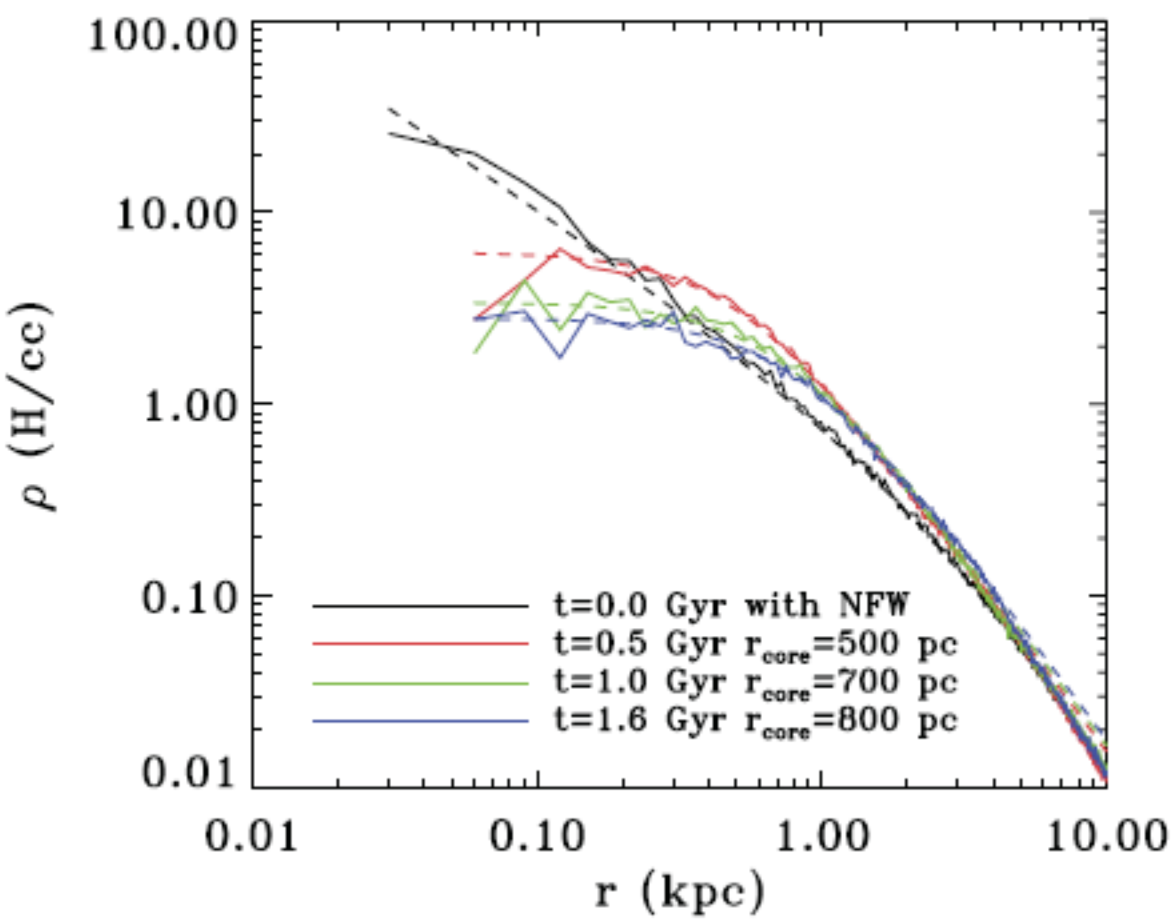

Figure 5. Evolution of the dark matter density profile over the 2Gyr of evolution for the control run with cooling, star formation and stellar feedback. We see the formation of a large core. We also show for comparison the analytical fit (dashed line) based on a pseudo-isothermal profile.

Romain Teyssier, Andrew Pontzen, Yohan Dubois and Justin I. Read 2013

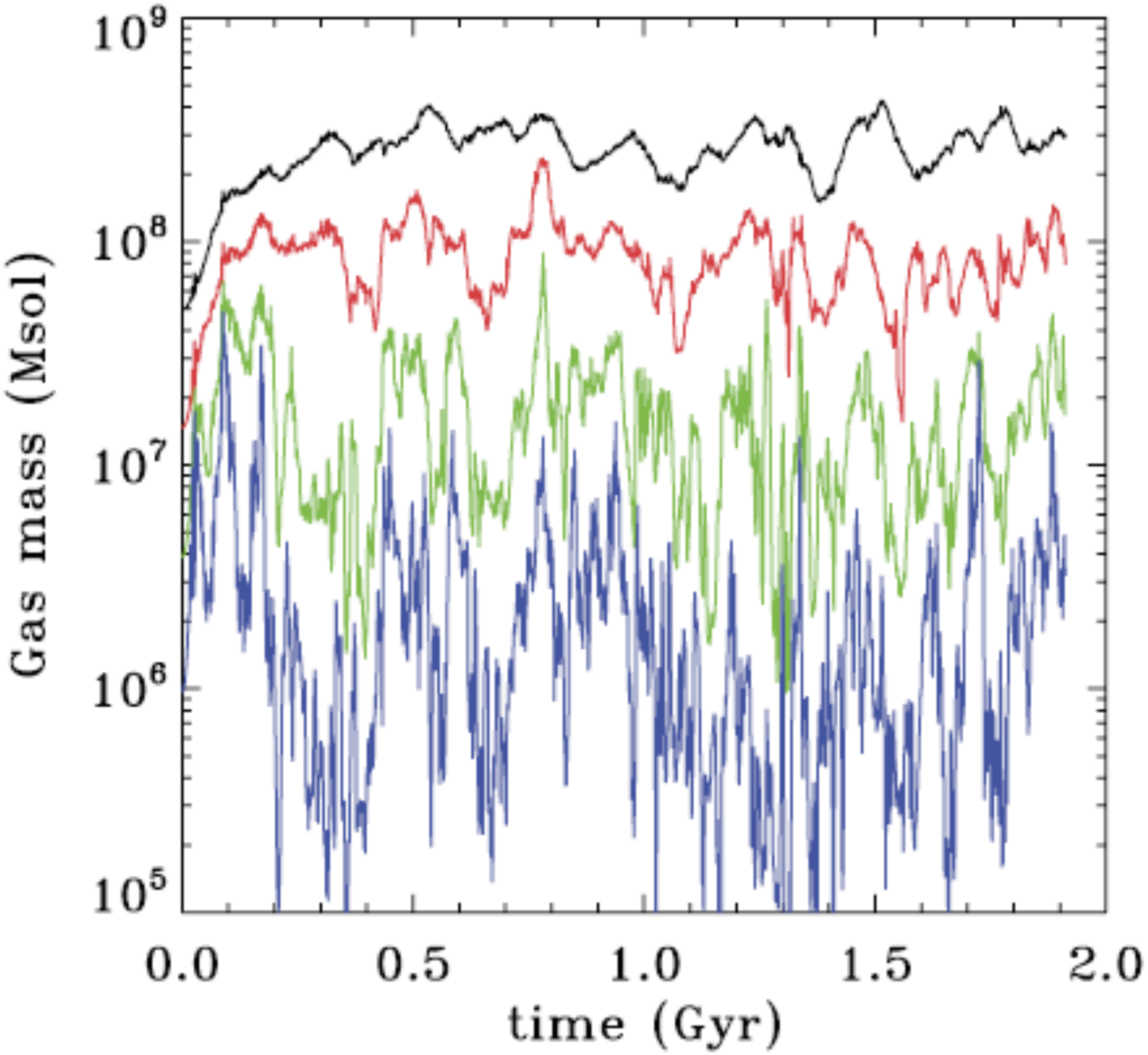

Figure 7. Time evolution of the total enclosed gas mass within spheres of radii 200 (blue), 400 (green), 800 (red) and 1600 (black) pc for the simulation with feedback.

Clumpy Disks

Fast accretion rate and slow rates of star formation lead to violent disk instabilities (VDI)

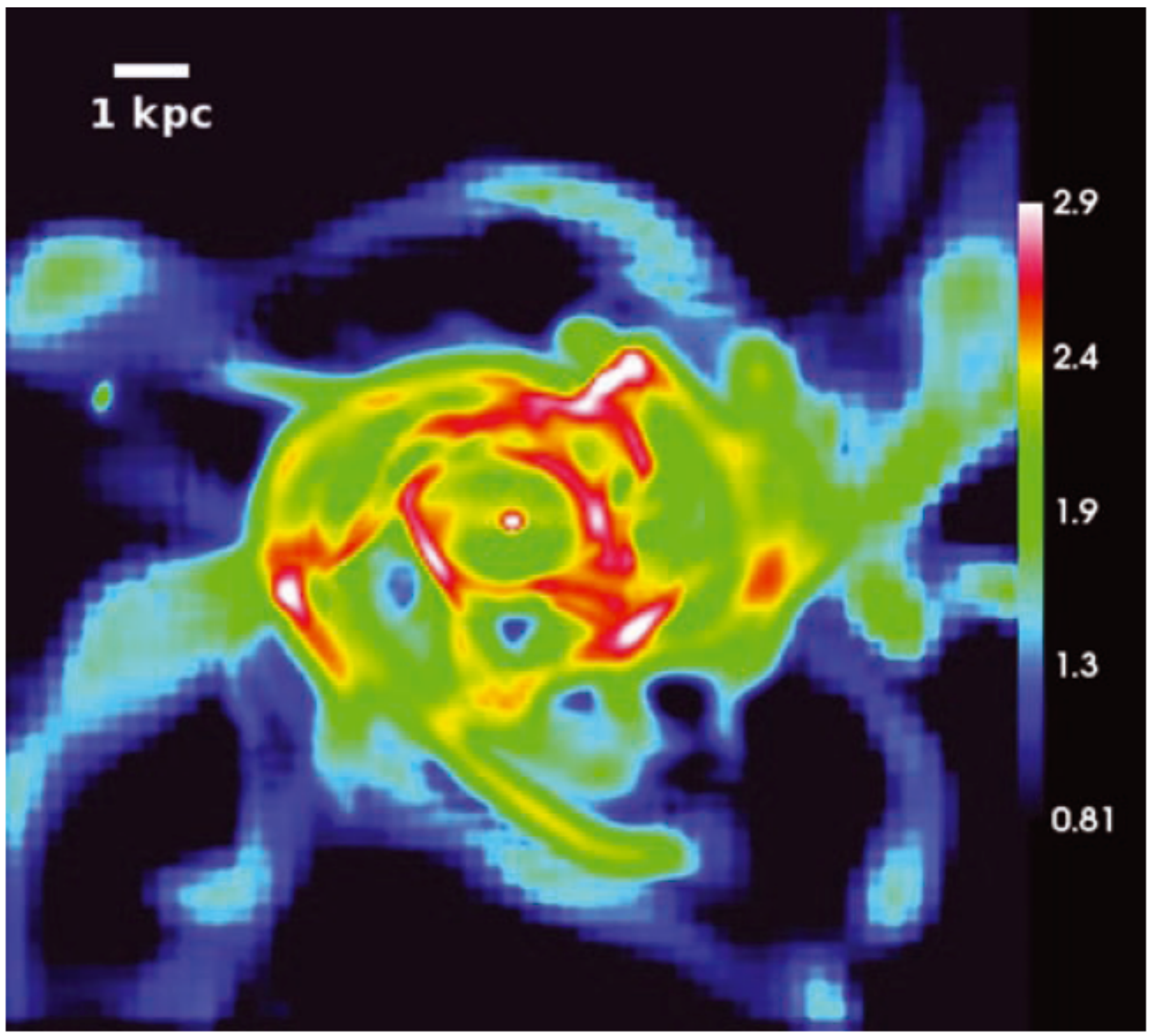

Figure 1. Face-on gas surface density in galaxy C at $z = 2.1$. The image demonstrates violent disc fragmentation into transient features and bound clumps, resembling observed SFGs and theoretical expectations. The size of the image is 15×15 kpc. Surface density is in units of $\log(\mathrm{M}_{\odot}\ \mathrm{pc}^{-2})$. For comparison, the surface density of molecular clouds in low-redshift galaxies is $\sim 100\,\mathrm{M}_{\odot}\ \mathrm{pc}^{-2}$.

Ceverino etal 2009

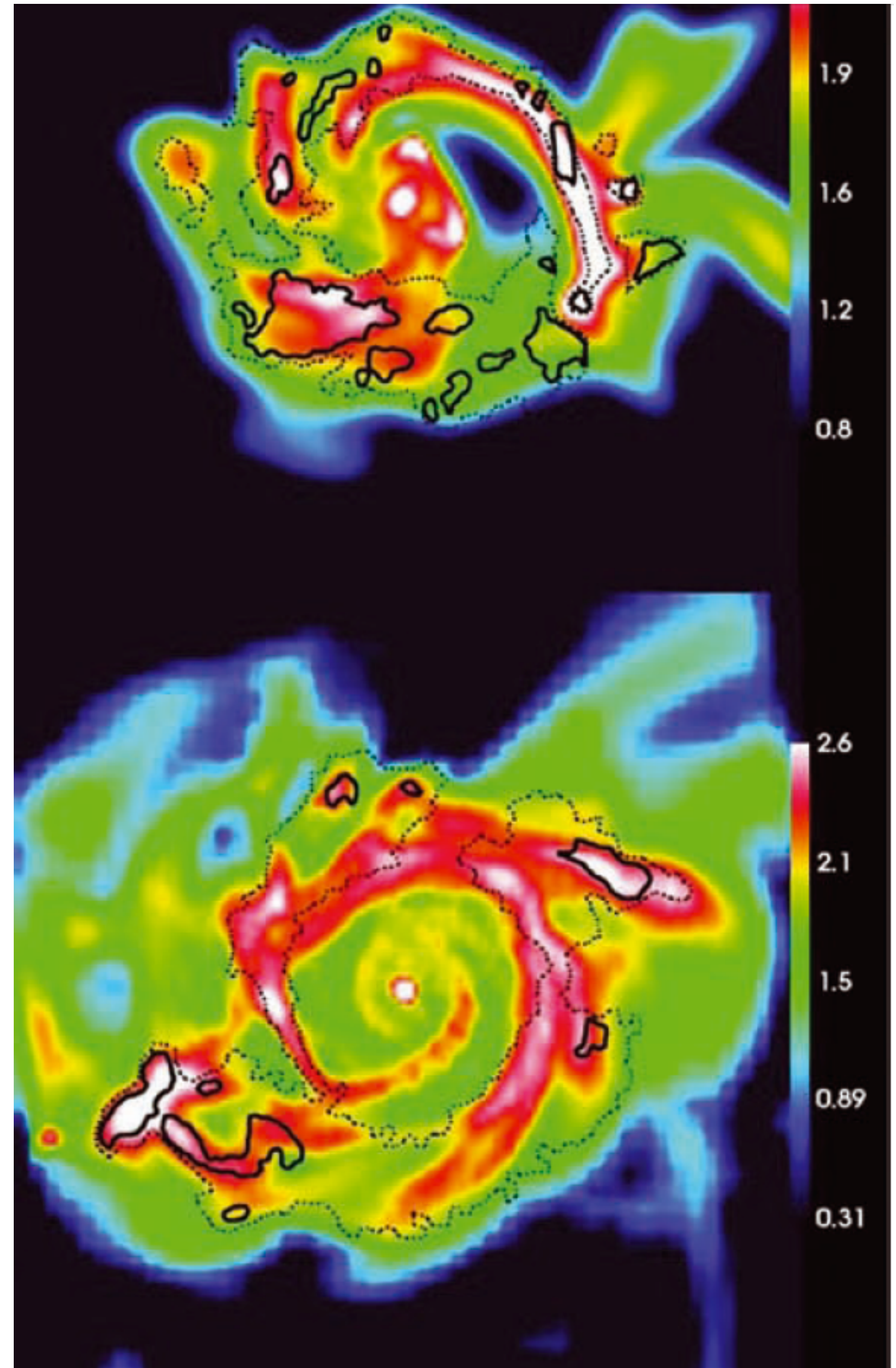

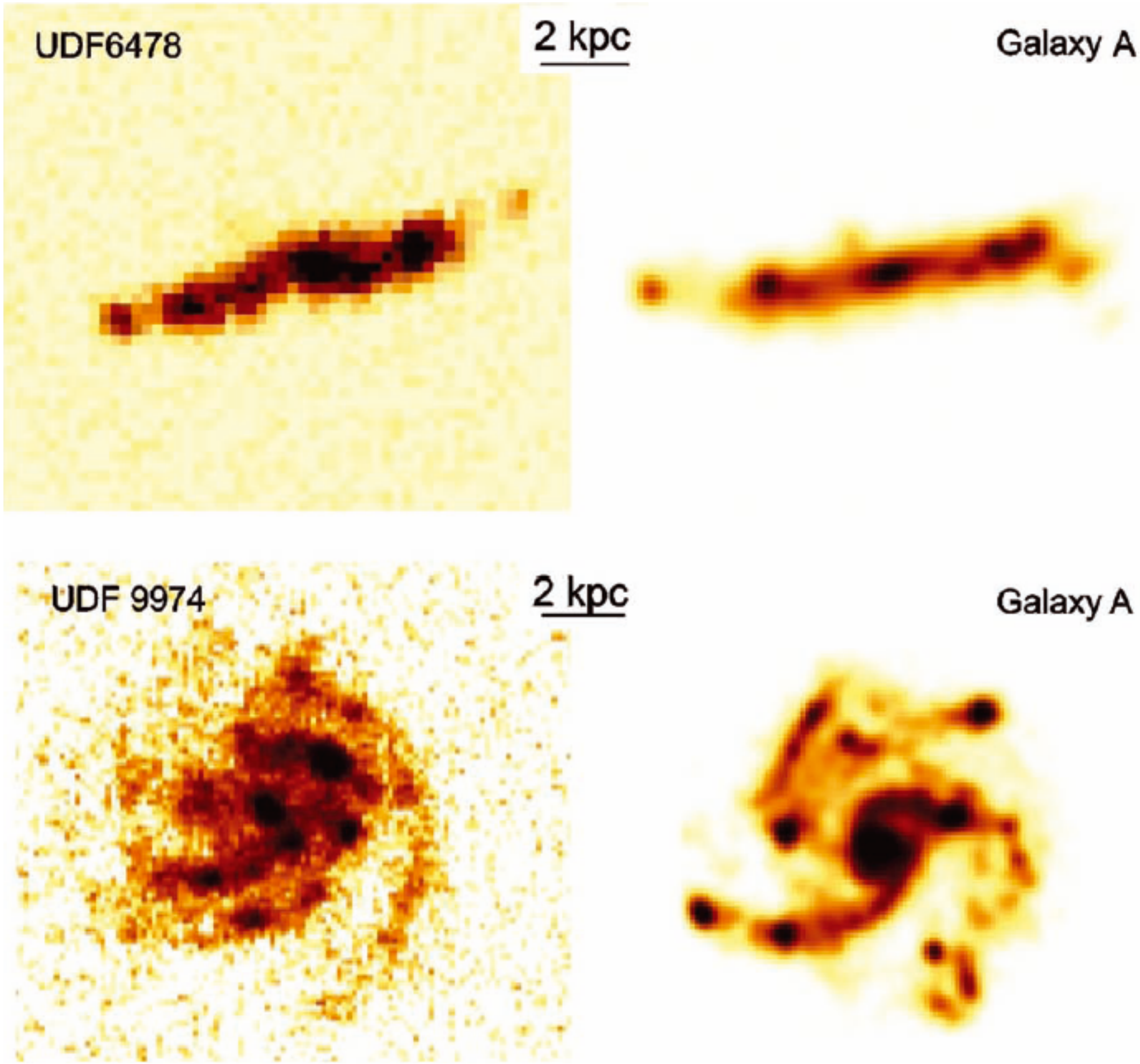
UDF6478
2 kpc
Galaxy A
UDF 9974
2 kpc
Galaxy A

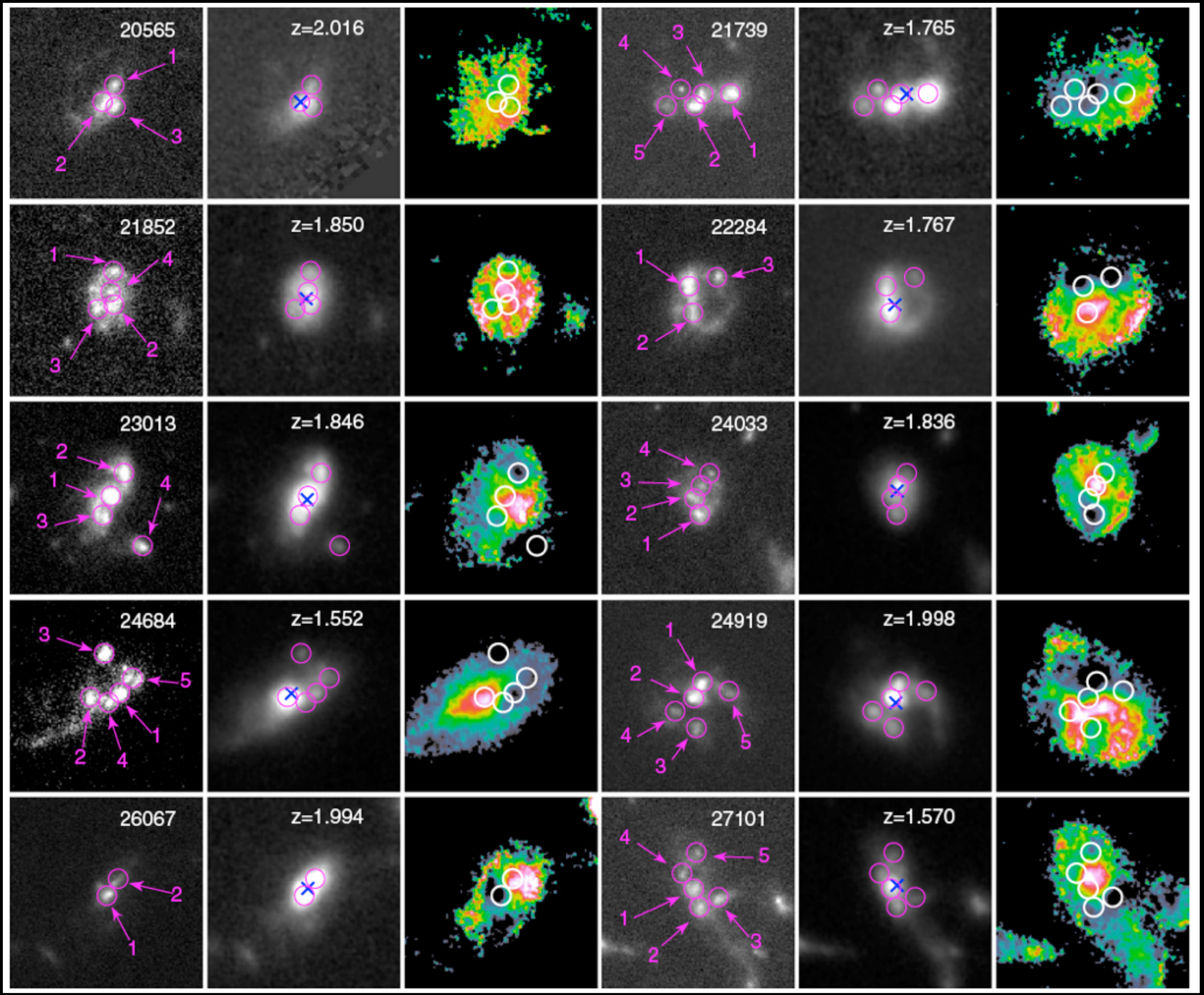

Montage of our 10 clumpy star-forming galaxies at $z \sim 2$. Each row shows images of two galaxies. For each galaxy, the panels from left to right show the z-band, H-band, and $z-H$ maps. Galaxy IDs are shown in the z-band images, while redshifts are shown in their H-band images. Small circles (magenta in the z-band and H-band images, and white in the $z-H$ maps) show the identified clumps. The blue "X"'s in the H-band images show the light-weighted centers.

Galaxy morphology at high z

Color–mass relation at $1.8 < z < 2.2$. The $U - V$ color is corrected for reddening. Objects detected at 24μm are shown as filled gray circles. The hatched region indicates the approximate 90% completeness limit for red-sequence objects at $z = 2$.

The color bar in the right panel shows the median sSFR as a function of dust-corrected color

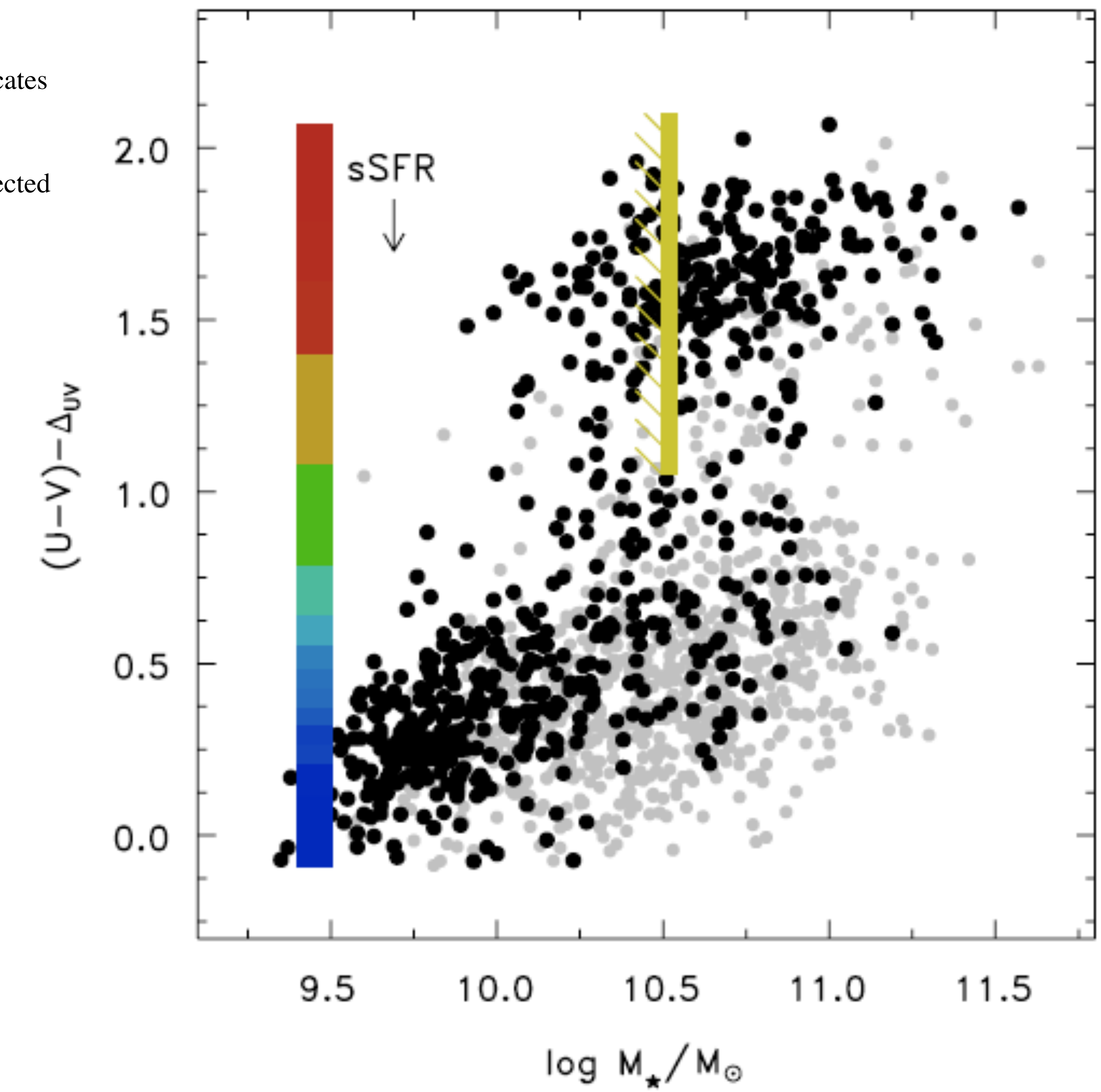

the cloud of galaxies with red dust corrected colors do, in fact, have very low sSFR.

The rest-frame U − V *color* distribution at all z=2.5 is bimodal, with a red peak, a blue peak, and a population of galaxies in between (the green valley).

We select 25,000 galaxies from the NEWFIRM Medium Band Survey (NMBS) to study the rest-frame $U - V$ color distribution of galaxies at $0 < z \; 2.5$. The five unique NIR filters of the NMBS enable the precise measurement of photometric redshifts and rest-frame colors for 9900 galaxies at $1 < z < 2.5$.

Brammer et al ApJ 706:L173–L177, 2009

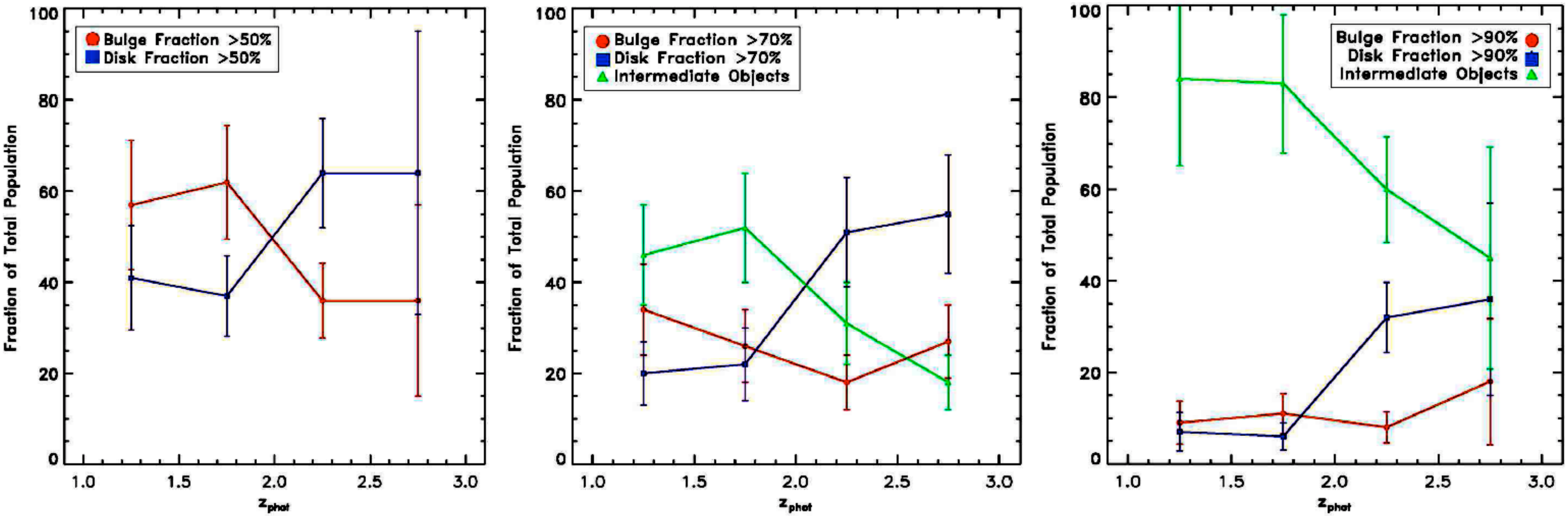

The redshift evolution of the morphological fractions in our galaxy sample, after binning into redshift bins of width z = 0.5 and using three alternative cuts in morphological classification

three alternative cuts in morphological classification as measured by B/T from bulge-disk decompositions.

In the left-hand panel of Fig. 1 we have simply split the sample into two categories: bulge-dominated (B/T > 0.5) and disk- dominated (B/T < 0.5).

In the central panel we have separated the sample into three categories, with any object for which 0.3 < B/T < 0.7 classed as “Intermediate”.

In the right-hand panel we have expanded this Intermediate category to encompass all objects for which 0.1 < B/T < 0.9.

z ≃ 2 marks a key transition phase, above which massive galaxies are predominantly disk-dominated systems and below which they become increasingly mixed bulge+disk systems.

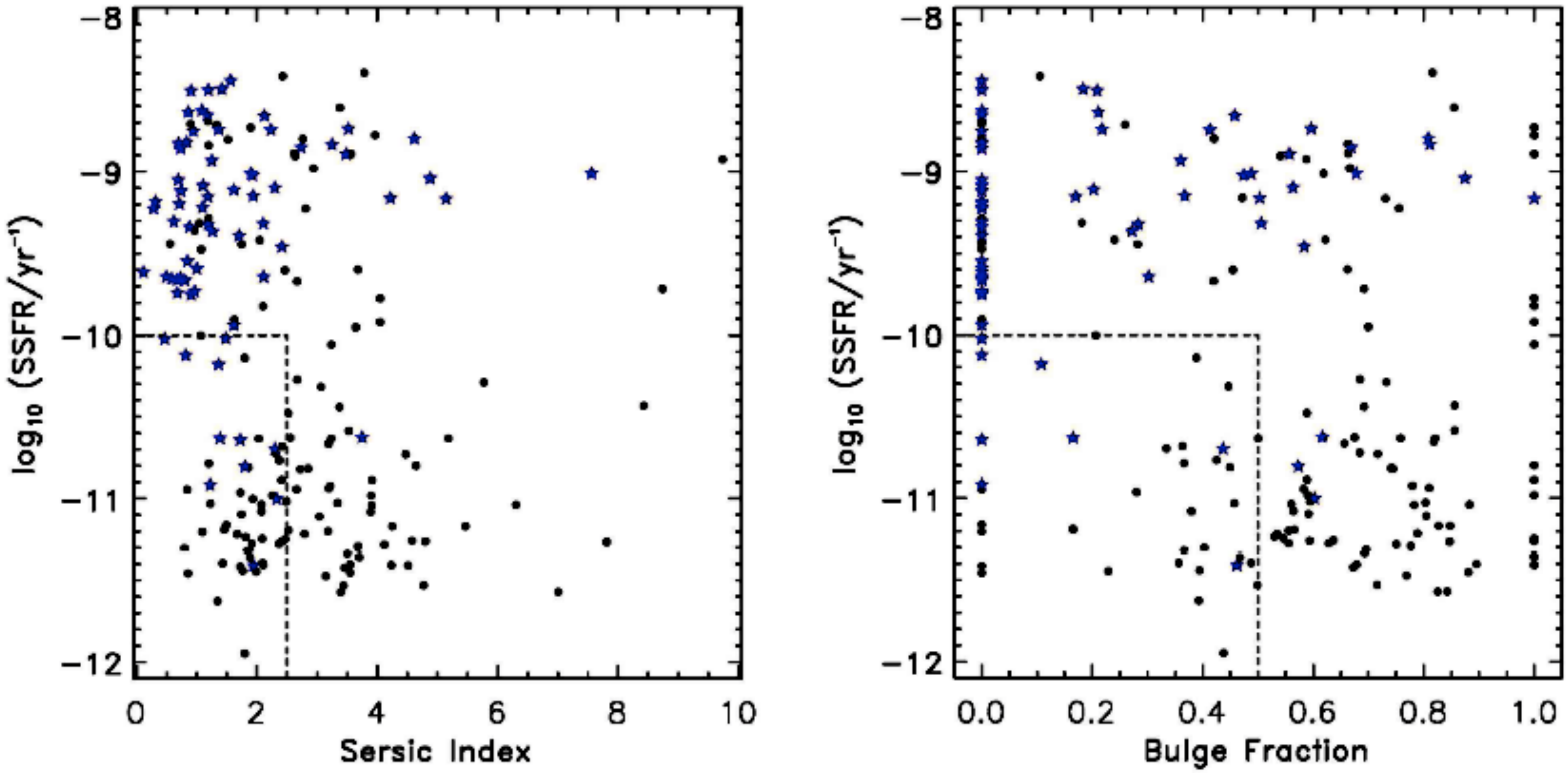

To first order, our results show that the well-documented bimodality in the colour-morphology plane seen at low redshift, where spheroidal galaxies inhabit the red sequence, while disk galaxies occupy the blue cloud is at least partly already in place by $z \simeq 2$.

Nonetheless, the sample also undoubtedly contains star-forming bulge-dominated galaxies and, perhaps more interestingly, a significant population of apparently quiescent disk-dominated objects.

Evolution of elliptical galaxies

Recent Structural Evolution of Early-Type Galaxies: Size Growth from $z=1$ to $z=0$
van der Wel etal 2008

Strong size and internal density evolution of early-type galaxies between $z\sim2$ and the present has been reported by several authors. Here we analyze samples of nearby and distant ($z\sim1$) galaxies with dynamically measured masses in order to confirm the previous, model-dependent results and constrain the uncertainties that may play a role. Velocity dispersion measurements are taken from the literature for 50 morphologically selected $0.8<z<1.2$ field and cluster early-type galaxies with typical masses 2e11 Msol. Sizes are determined with ACS imaging. We compare the distant sample with a large sample of nearby ($0.04<z<0.08$) early-type galaxies extracted from the SDSS for which we determine sizes, masses, and densities in a consistent manner, using simulations to quantify systematic differences between the size measurements of nearby and distant galaxies. We find a highly significant structural difference between the nearby and distant samples, regardless of sample selection effects. The implied evolution in size at fixed mass between $z=1$ and the present is a factor of 1.97(0.15). This is in qualitative agreement with semianalytic models; however, the observed evolution is much faster than the predicted evolution. Our results reinforce and are quantitatively consistent with previous, photometric studies that found size evolution of up to a factor of 5 since $z\sim2$. A combination of structural evolution of individual galaxies through the accretion of companions and the continuous formation of early-type galaxies through increasingly gas-poor mergers is one plausible explanation of the observations.

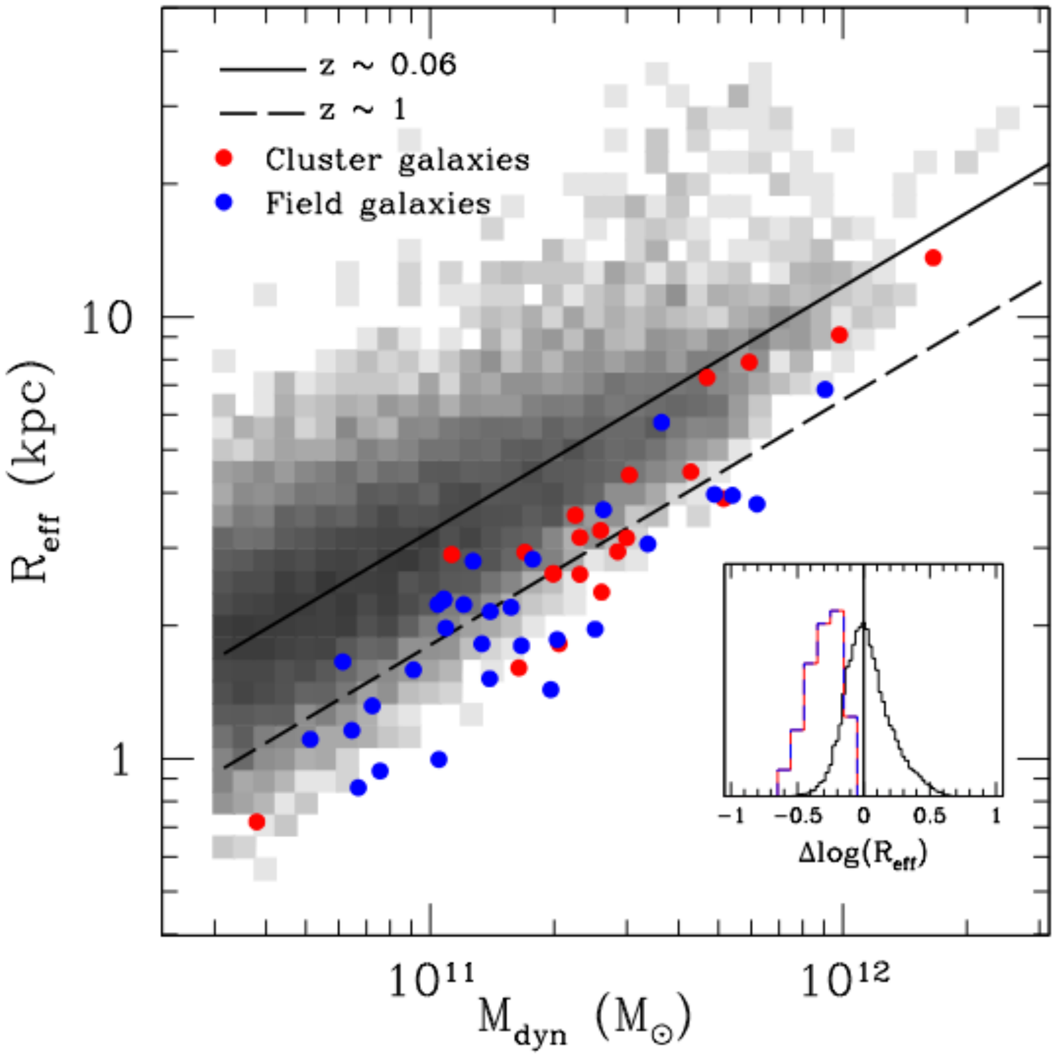

FIG. 4.— Mass-size relation for the nearby sample (*solid line*) and at $z \sim 1$ (*dashed line*); the symbols are the same as in Fig. 3. For the derivation of the M_{dyn}-R_{eff} relation for the nearby sample see § 2.2; for the derivation of the M_{dyn}-R_{eff} relation for the distant sample see § 5.2. The smaller, inset panel shows the distribution of the two samples around the M_{dyn}-R_{eff} relation of the nearby sample (*the solid line in the large panel*). The distant galaxies are 1.8 ± 0.1 times smaller than the nearby galaxies. It appears that the most massive galaxies do not show as large an offset. This indicates that size evolution may be slower for the highest mass galaxies than for low-mass galaxies, but it has to be kept in mind that these very massive galaxies are brightest cluster galaxies and may therefore have developed differently from other galaxies.

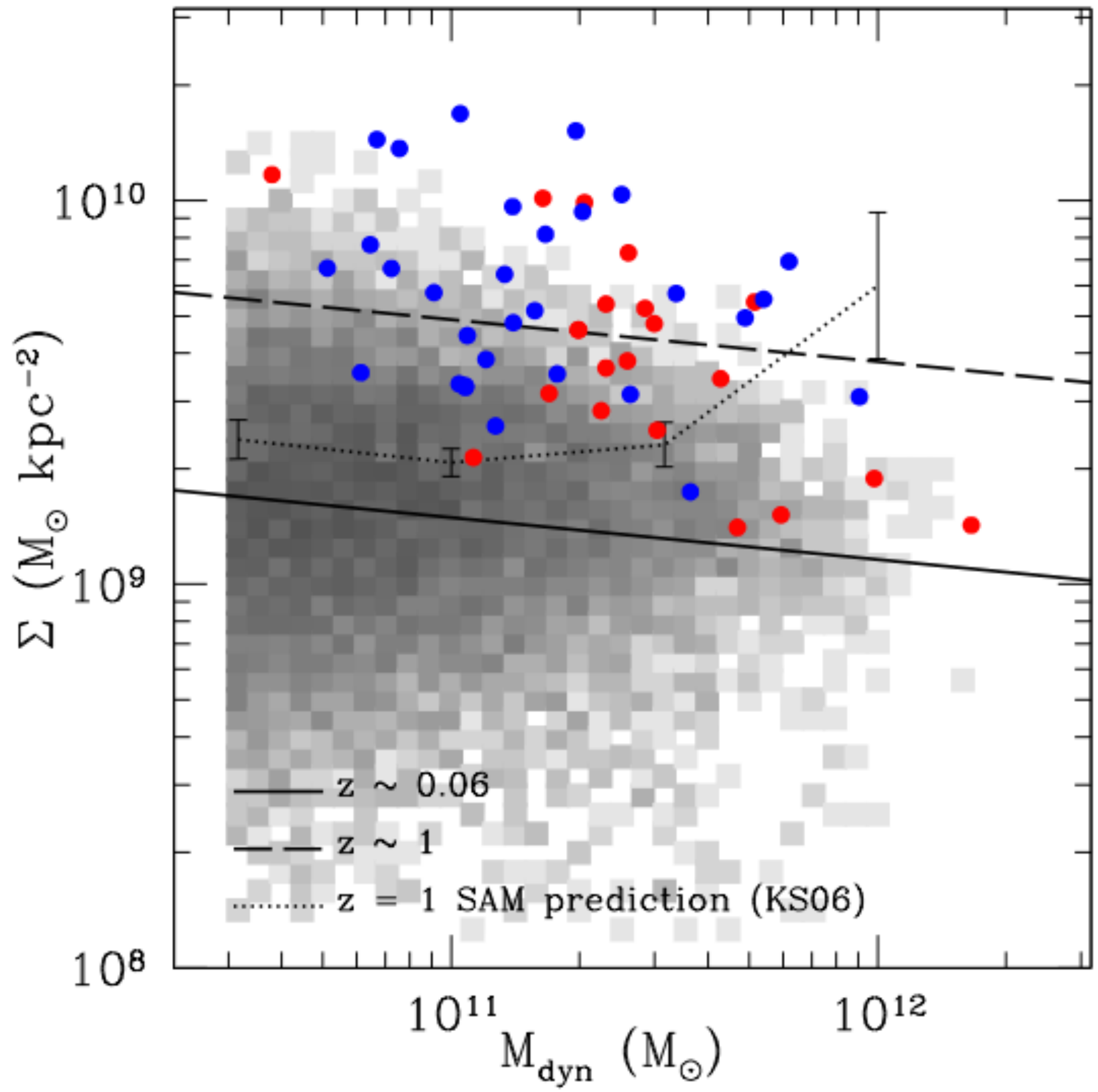

FIG. 5.— Mass-density relation at $z \sim 1$. The symbols and lines are the same as in Figs. 3 and 4. The $z \sim 1$ early-type galaxies are ~ 4 times more dense than their nearby counterparts. The prediction of the semianalytic size-evolution model for elliptical galaxies from Khochfar & Silk (2006a) is shown as the dotted line. The error bars indicate the predicted size evolution between $z = 0.8$ and $z = 1.2$, the redshift range of our distant sample. Despite qualitative agreement, there are significant quantitative differences between the predicted and observed evolution.

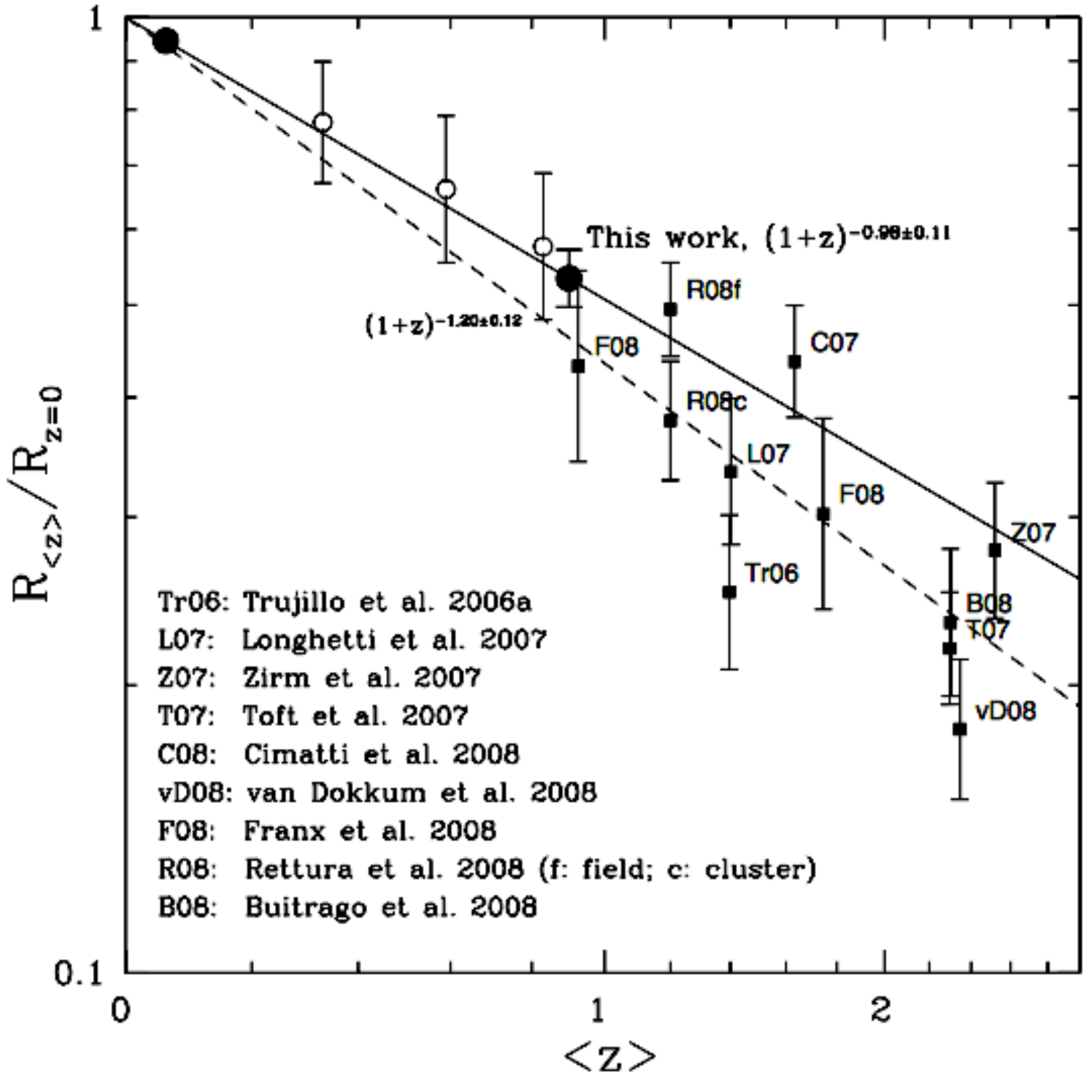

FIG. 6.— Size evolution with redshift as derived in this paper with dynamically determined masses (*large filled circles*) compared with previous results based on photometric masses (*small filled circles*). The solid line connects our samples at $z \sim 0.06$ and $z \sim 1$, the dashed line is a linear least-squares fit to the small filled data points. The open circles are samples of cluster galaxies with photometrically measured masses and serve as an illustration that size evolution shows a continuous trend between $z = 2.5$ and the present. The broad agreement in size evolution as derived from galaxies with dynamically and photometrically determines masses reinforces the conclusions of previous, photometric studies whose results were potentially mitigated by considerable systematic effects that do not affect our analysis.

ual galaxies. Numerical simulations have demonstrated that when early-type galaxies accrete neighbors without significant dissipational processes $\sigma_{\rm eff}$ does not change by much and that, to first order, $R_{\rm eff}$ increases linearly with mass. This does not depend strongly on the mass of the accreted object, i.e., the mass ratio of the merger (Boylan-Kolchin et al. 2005; Robertson et al. 2006; Boylan-Kolchin et al. 2006).

Simulations in a cosmological context show that an increase in size by a factor of 2 between $z \sim 1$ and the present is certainly possible (Naab et al. 2007). The strong observed size evolution thus argues in favor of a scenario in which significant mass from low-mass companions is accreted onto existing early-type galaxies over the past ~7 Gyr, which also explains the broad tidal features that are frequently observed around early-type galaxies (van Dokkum 2005). As shown by Feldmann et al. (2008) such features are not necessarily, and are even quite unlikely to be, the result of major merger events and are most likely due to the accretion of low-mass, gas-poor satellites.